Tensor networks and Matrix product states to study quantum properties of multipartite systems

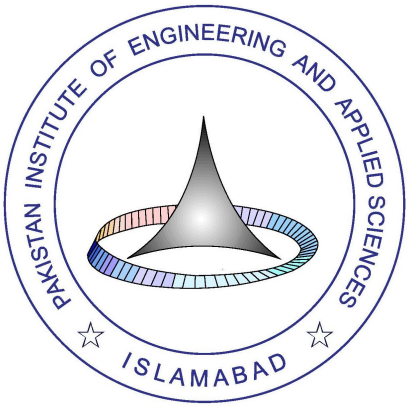

Saad Qasim Abbasi

2023

Department of Physics and Applied Mathematics Pakistan
Institute of Engineering and Applied Sciences
Nilore, Islamabad, Pakistan

This page is intentionally left blank.

Certificate of Approval

This is to certify that the work contained in this thesis entitled **Tensor networks and Matrix product states to study quantum properties of multipartite systems**, was carried out by **Saad Qasim Abbasi**, and in my opinion, it is fully adequate, in scope and quality, for the degree of **Bachelors**. Furthermore, it is hereby approved for submission for review and thesis defense.

Supervisor: _____

Name: **Dr. Muhammad Irfan**
Date: 25 July, 2023
Place: PIEAS, Islamabad

Co-Supervisor: _____

Name: **Dr. Shahid Qamar**
Date: 25 July, 2023
Place: PIEAS, Islamabad

Head, DPAM: _____

Name: **Dr. Shakeel ur Rehman**
Date: 25 July, 2023
Place: PIEAS, Islamabad

Tensor networks and Matrix product states to study quantum properties of multipartite systems

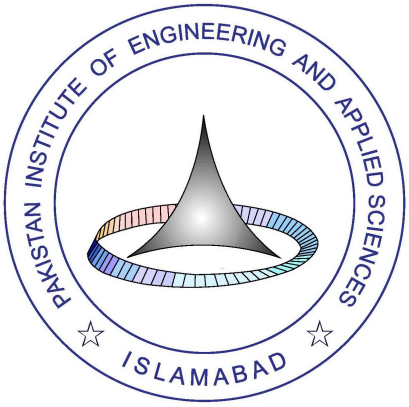

Saad Qasim Abbasi

Submitted in partial fulfillment of the requirements
for the degree of BS Physics.

2023

Department of Physics and Applied Mathematics
Pakistan Institute of Engineering and Applied Sciences
Nilore, Islamabad, Pakistan

Dedications

I wholeheartedly dedicate this thesis to the unwavering support and love of my parents, whose encouragement and sacrifices have been my guiding light throughout this journey. I am deeply grateful to my dedicated advisor, Muhammad Irfan, for his invaluable guidance and expertise. Lastly, I extend my heartfelt appreciation to the Department of Physics and Applied Mathematics for providing a nurturing environment that fostered my intellectual growth and academic pursuits.

Declaration of Originality

I hereby declare that the work contained in this thesis and the intellectual content of this thesis are the product of my work. This thesis has not been previously published in any form nor does it contain any verbatim of the published resources which could be treated as infringement of the international copyright law. I also declare that I do understand the terms 'copyright' and 'plagiarism,' and that in case of any copyright violation or plagiarism found in this work, I will be held fully responsible for the consequences of any such violation.

Saad Qasim Abbasi

Date:

Place: PIEAS, Islamabad

Acknowledgments

Copyrights Statement

Contents

Abstract

This thesis explores the fascinating realm of Tensor Networks and their application to pulse propagation through atomic ensembles in the context of the Vacuum Induced Transparency (VIT) setting. Tensor Networks offer a powerful framework for representing and manipulating complex quantum states, providing a bridge between quantum information theory and condensed matter physics. The study begins with a comprehensive review of the fundamental principles underlying Tensor Networks, including the concept of entanglement and the role Tensor Networks play in efficiently truncating the exponentially growing Hilbert space. Furthermore, the groundwork is laid for understanding Matrix Product States and their relation to one-dimensional quantum systems. Drawing inspiration from the seminal paper on pulse propagation through atomic ensembles using MPS [1], we study and analyse the intricate dynamics of light-matter interactions in the VIT regime. This thesis investigates the impact of quantum jumps and multi-photon wavepacket distortion on observed delay times as they enter a medium, resulting in variations in photon arrival times at the atomic ensemble's boundary. This provides the characteristic delay of input photon number for VIT. The study employs MPS and Tensor Network techniques for numerical simulations, enriching the understanding of the system's behavior in quantum physics research. These significant findings have implications for experimental setups and contribute to the advancement of our knowledge of quantum phenomena.

Chapter 1

Introduction

The curse of dimensionality presents a major challenge in investigating quantum many-body systems, as it entails the exponential growth of the Hilbert space, making efficient description and study of states difficult. However, it is worth noting that certain physically relevant states exhibit additional structure, not present in arbitrary states. This distinguishing feature allows for their efficient description and study, thereby circumventing the complexity barrier posed by the curse of dimensionality. Tensor networks, apart from their application in many-body physics, also offer insights into fundamental concepts in quantum information. By utilizing the tensor network framework, one can gain a relatively simple understanding of concepts such as quantum teleportation, purification, and quantum circuit optimization etc.

1.1 Motivation for Tensor Networks

Quantum Mechanics, being inherently complex, can be aptly characterized by Dirac's statement: "The fundamental laws required for the mathematical treatment of a significant portion of physics and the entirety of chemistry are already fully understood. The challenge lies in the fact that applying these laws leads to equations that are too intricate to solve" [2]. Irrespective of the specific system under consideration, such as a collection of spins or particles, if the wavefunction encompasses numerous components, it becomes a high-dimensional entity, necessitating exponential complexity to describe and solve the associated Schrödinger equation. Consequently, the Schrödinger equation cannot be exactly solved for systems comprising more than ten particles or so, leading to the notion that the wavefunction of many-electron systems is not a scientifically practical concept. However, its apparent complexity is illusory. In the particular context of the Hamiltonians and energy scales present in our physical reality, nature does not

explore the entire Hilbert space. As a result, there are inherent constraints on the types of quantum states that naturally occur. Due to the specific structure of most physical quantum states, the exponential complexity does not manifest. A key example of such a restriction is locality, which implies that a system's response is localized. Consequently, the ground states, constituting the low energy scale, exhibit low entanglement. This characteristic is mathematically proven in gapped systems in one dimension [3] and can be argued to hold true in gapless systems in one dimension and higher dimensions as well. Tensor Networks offer a viable approach to dealing with these physically relevant quantum states characterized by low entanglement. Various types of Tensor Networks correspond to different entanglement geometries. For instance, Matrix Product State (MPS) addresses one-dimensional entanglement in gapped systems and serves as the foundation for Density Matrix Renormalization Group (DMRG) techniques [4]. Projected Entangled Pair States (PEPS) are designed to handle two-dimensional entanglement, while Multiscale Entanglement Renormalization Ansatz (MERA) is suitable for handling one-dimensional and multi-dimensional entanglement in both gapless and critical systems.

1.2 Limitations of current simulation techniques

The existence of numerous numerical techniques for studying strongly correlated systems may lead one to question the necessity of tensor network (TN) methods. While this is a valid inquiry, it lacks a straightforward answer. Nevertheless, there are compelling reasons to highlight the importance and indispensability of TN methods. Alternative numerical approaches, such as exact diagonalization (e.g. Lanczos methods [5]), series expansion techniques [6], mean field theory [7], quantum Monte Carlo algorithms [8], continuous unitary transformations [9], coupled cluster methods [10], and density functional theory [11], each possess inherent limitations. For instance, exact diagonalization is confined to small systems that are far from the thermodynamic limit where quantum phase transitions occur. Series expansion techniques rely on perturbation theory calculations, while mean field theory fails to accurately account for quantum correlations. Quantum Monte Carlo algorithms encounter the sign problem, restricting their applicability to fermionic and frustrated quantum spin systems. Continuous unitary transformations require approximations for solving a system of infinitely-many coupled differential equations, and coupled cluster methods are primarily applicable to small and medium-sized molecules. Density functional theory heavily relies on the modeling of exchange and correlation interactions among electrons, among other

factors. These examples merely scratch the surface of the limitations associated with these approaches. However, TN methods also have their own limitations. The primary constraint lies in the amount and structure of entanglement present in quantum many-body states. This computational method introduces a new set of challenges that extend the range of difficulties encountered in computational physics. TN methods offer a distinct approach to representing quantum states as networks composed of interconnected tensors. This unique representation enables the accurate characterization of relevant entanglement properties, surpassing the capabilities of traditional approaches that rely solely on wavefunction coefficients in a given basis. In the case of TN states, complex equations can be transformed into intuitive tensor network diagrams. This visual language for describing quantum states of matter, encompassing phenomena that go beyond the conventional framework established by Landau [12], such as quantum spin liquids [13] and topologically-ordered states [14], has been recognized as a groundbreaking development in condensed matter physics and quantum physics at large. The visual representation of quantum states through tensor networks stimulates new intuitions, ideas, and discoveries, making it an invaluable tool for researchers in these fields.

1.3 An investigation into the application of Matrix Product States technique for pulse propagation in Vacuum-Induced Transparency:

In the realm of quantum physics, the phenomenon of vacuum-induced transparency (VIT) has emerged as a captivating area of research. VIT is closely related to electromagnetically induced transparency (EIT), a phenomenon that occurs in three-level atomic media. It offers intriguing possibilities for manipulating light and its propagation properties [15]. VIT arises when a coherent optical pulse interacts with a medium, resulting in a reduction in its absorption and enhanced group velocity. Exploiting this phenomenon holds great potential for the development of novel technologies, including quantum information processing, quantum communication, and precision measurement systems. The investigation of pulse propagation in the context of vacuum-induced transparency necessitates the exploration of advanced computational techniques capable of accurately modeling the intricate dynamics of quantum systems. In recent years, the Matrix Product States (MPS) technique has gained significant attention and recognition for its remarkable ability to describe and simulate the behavior of quantum many-body

systems. The MPS approach offers a powerful framework for efficiently representing and manipulating quantum states, enabling the study of complex interactions and phenomena with unprecedented precision. The primary objective of this thesis is to delve into the realm of pulse propagation in vacuum-induced transparency, employing the MPS technique as a computational tool for unraveling the underlying dynamics. By harnessing the capabilities of MPS, we aim to investigate the intricate interplay between the optical pulse and the medium, shedding light on the mechanisms governing VIT and its potential applications. To achieve this objective, we will construct a theoretical framework that combines the principles of quantum optics, the theory of pulse propagation, and the MPS formalism. Through a comprehensive analysis of the governing equations and fundamental concepts, we will develop a robust computational model capable of accurately simulating the behavior of quantum systems under various VIT conditions.

1.4 Thesis Layout

The thesis is structured into several chapters, each exploring different aspects of the research topic. Chapter 2 focuses on entanglement, geometry, and exponential Hilbert space. It introduces the concept of entanglement and its connection to exponential Hilbert space, providing a foundation for further exploration. The chapter also discusses tensor network theory, MPS and Matrix Product Operator (MPO). It covers compression algorithms for MPS, energy optimization techniques, time evolution, and the role of symmetries. In Chapter 3, the focus shifts to tensor network renormalization. The chapter delves into the application of renormalization group (RG) to the quantum Ising model and explores the elimination of short-range interactions through renormalization. Additionally, it introduces the multi-scale entanglement renormalization ansatz (MERA) and its connection to holography. Chapter 4 investigates the simulation of quantum light using MPS. It explores strong interactions and many-body phenomena in photon-atom ensembles, along with the simulation of a 1D spin model for light propagation. The chapter employs MPS and methods such as the quantum jump formalism and time evolution with MPS. The simulation of vacuum-induced transparency is also discussed. Finally, Chapter 5 presents the results and discussion of the research findings. It concludes the thesis by summarizing the key outcomes and providing an analysis of the obtained results. The thesis concludes with a section for references and an appendix.

Chapter 2

Theoretical background of Tensor Network

2.1 Entanglement, Geometry and exponential Hilbert space

The task of discerning the structure of entanglement within a quantum many-body wavefunction based solely on the coefficients in a local basis is often challenging. The nature of entanglement structure can vary depending on factors such as the system's dimensionality, criticality, and correlation length.Therefore finding a quantum state representation that preserves the explicit and accessible knowledge of entanglement structure is thus desirable.

Tensor network (TN) states offer a unique capability to provide direct and explicit information regarding the structure of entanglement through their representation as networks of quantum correlations. In essence, TN states can be thought of as quantum states that are represented by entanglement, with several representations designed for various sorts of states, such as 1D, 2D, or critical states. The effective lattice geometry in which the state occurs can be determined thanks to the network of correlations present in TN states. Additionally, it has been proposed in a number of publications that the pattern of entanglement existing in quantum states could naturally give rise to geometry, curvature, and gravity [16]. Although a detailed exploration of this concept is beyond the scope of this discussion, it becomes clear that the language of TN is ideally suited for exploring such linkages, making it an exciting and promising area for research. The immense dimensionality of the Hilbert space, which exponentially expands with the number of particles, is the primary reason why TNs are necessary for modelling quantum many-body states in nature. It is ineffective to only use the

coefficients in a local basis to represent a quantum state of a many-body system. Quantified by the number of basis states in the Hilbert space, the quantum states in a quantum many-body system are extremely many. For instance, the number of basis states in the Hilbert space reaches a stunning value of $\mathcal{O}(10^{10^{23}})$, exceeding the number of atoms in the observable universe, when N is roughly on the order of 10^{23} (similar to Avogadro's number). Fortunately, not every quantum state in a many-body system's Hilbert space is equally important.

In many crucial Hamiltonians found in nature, the interactions between particles tend to be local. This locality of interactions carries significant implications, such as establishing that low-energy eigenstates of gapped Hamiltonians with local interactions adhere to the area-law for entanglement entropy. This remarkable property implies that, for sufficiently large regions, the entanglement entropy of a space region scales with the size of its boundary rather than its volume [3]. This result exclusively applies to states satisfying the area-law and only those states can be valid candidates for low-energy states of a gapped, local Hamiltonian. The manifold encompassing these states represents an exponentially small portion within the vast Hilbert space. To investigate states within this manifold, a tool is required to target it directly instead of considering the entire Hilbert space. TN states form a family of states precisely designed to capture this most relevant corner of states, making it natural to develop Renormalization Group (RG) methods based on TN states to address this essential segment of quantum states. Moreover, the Hilbert space is so immense that even evolving a quantum many-body state for a time complexity of O(poly(N)) with a local Hamiltonian, the majority of the Hilbert space remains practically inaccessible. For instance, for a system of N$\sim 10^{23}$ particles, evolving a quantum state with a local Hamiltonian to reach most states in the Hilbert space would take approximately $\mathcal{O}(10^{10^{23}})$ seconds, far surpassing the age of the universe [17]. Therefore, it is essential to concentrate on the pertinent area of quantum states rather than taking into account the complete Hilbert space.

2.2 Tensor Network theory:

Next we delve into the mathematical concepts related to tensor network (TN) states and their representation using TN diagrams. We will introduce the TN representation of quantum states and discuss two prominent examples: MPS for 1D systems and Projected Entangled Pair States (PEPS) for 2D systems. In the context of our discussion, a tensor refers to a multidimensional array consisting of complex numbers. The rank of a tensor corresponds to the number of indices it

possesses. For instance, a rank-0 tensor is a scalar represented by a single complex number (x). A rank-1 tensor is a vector denoted by its components (v_α), where α represents the index running over the dimensions of the vector. Similarly, a rank-2 tensor is a matrix characterized by two indices ($A_{\alpha\beta}$) spanning the rows and columns of the matrix. For instance, the matrix product $C_{\alpha\gamma} = \sum_{\beta=1}^{D} A_{\alpha\beta}B_{\beta\gamma}$ is the contraction of index β, which amounts to the sum over its D possible values. One can also have more complicated contractions, such as this one:

$$F_{\gamma\omega\rho\sigma} = \sum_{\alpha,\beta,\delta,\nu,\mu=1}^{D} A_{\alpha\beta\delta\sigma}B_{\beta\gamma\mu}C_{\delta\nu\mu\omega}E_{\nu\rho\alpha} \tag{2.1}$$

where for simplicity we assumed that the contracted indices ν, μ, α, β, and δ may each have D distinct values. As seen by these examples, the contraction of indices results in the creation of new tensors, much as the creation of a new matrix by multiplying two matrices. An index contraction occurs when we sum over all possible values of repeated indices within a set of tensors. This operation is denoted by connecting the repeated indices with a summation symbol. The summation is performed over the entire range of values for each repeated index, and the result yields a new tensor with reduced rank. This process allows for the consolidation of indices and facilitates calculations involving tensors. Index contractions play a crucial role in various tensor operations, such as matrix multiplication, tensor contractions, and the manipulation of higher-rank tensors. They enable the combination of tensor components and the extraction of meaningful information from the data stored in tensors. By performing index contractions, we can exploit the algebraic properties of tensors and uncover relationships between different components of the tensors involved.

Using tensor network diagrams, as shown in Fig. 2.1, it is now useful to propose a diagrammatic notation for tensors and tensor networks . Tensors are shown in these diagrams as shapes, and the indices within the tensors are shown as lines coming out of the shapes.

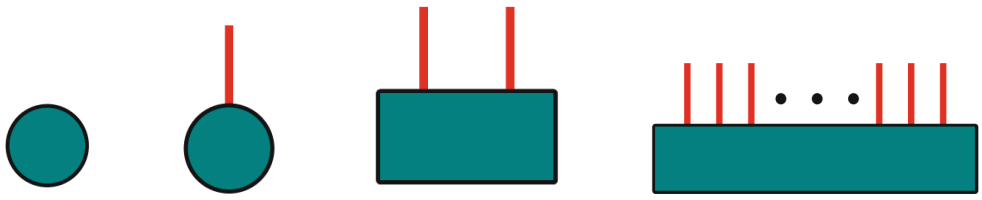

Figure 2.1: Scalar, vector, matrix, and Rank-3 tensor diagrams of tensor networks are shown from left to right.

The diagrammatic notation provides a visual representation of the tensor net-

work, making it easier to grasp and analyze the structure and connectivity of the network. The shapes in the diagram correspond to the tensors involved, and the lines represent the indices of those tensors. The lines that connect different tensors indicate that the corresponding indices are contracted or summed over, while the lines that do not connect to other tensors indicate open or uncontracted indices. By utilizing tensor network diagrams, one can easily visualize the flow of indices and identify the contracted and open indices within the TN. A few examples of such contractions are shown in Fig. 2.2. This diagrammatic representation simplifies the understanding and manipulation of tensor networks, facilitating calculations and derivations involving complex tensor operations.

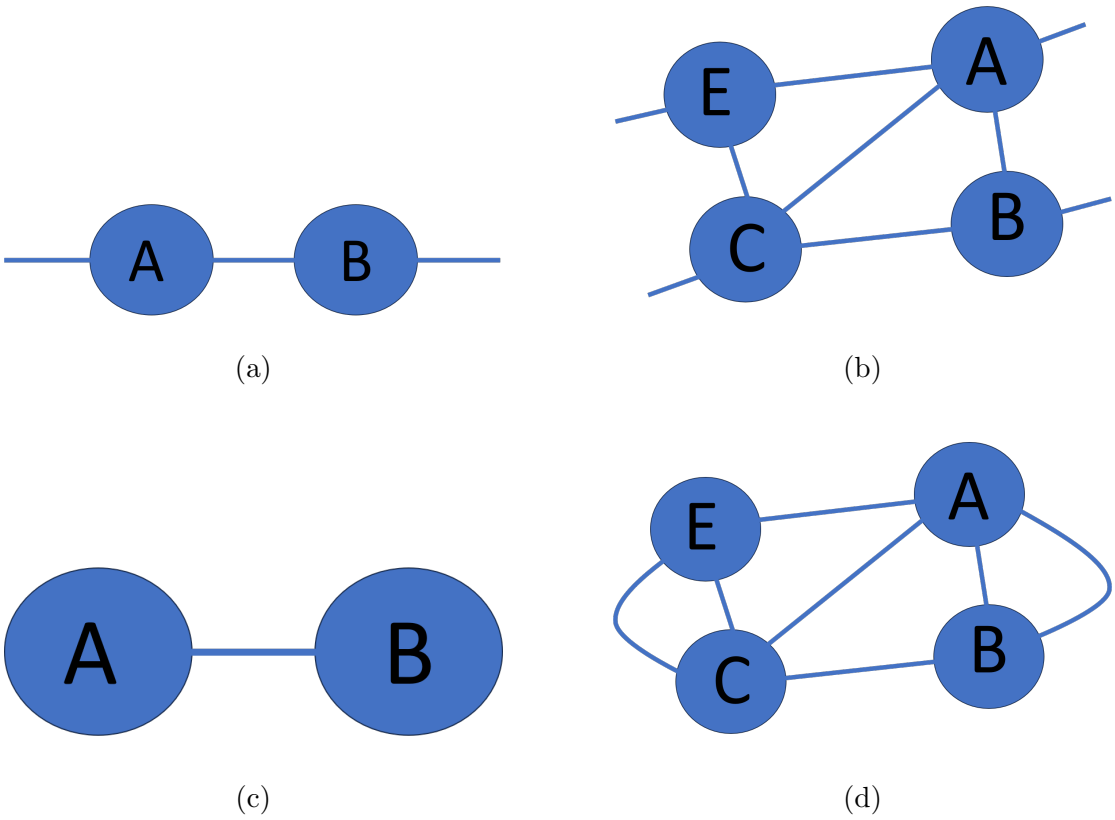

Figure 2.2: Tensor network diagrams (a) matrix product, (b) contraction of 4 tensors with 4 open indices, (c) scalar product of vectors, and (d) contraction of 4 tensors without open indices.

In the TN representation, we encounter two noteworthy examples. First, MPS are employed to describe 1D systems. In an MPS, the wavefunction is expressed as a product of matrices, where each matrix corresponds to a specific site or particle in the system as shown in Fig. 2.3. The matrices capture the entanglement between neighboring particles, enabling an efficient representation of 1D quantum states. Second, Projected Entangled Pair States (PEPS) are utilized for 2D systems. PEPS employ tensors to describe the quantum state of a 2D lattice as

shown in Fig. 2.4. Each tensor represents the local degrees of freedom associated with a lattice site, while the interconnections between tensors encode the entanglement between neighboring sites. PEPS provide a powerful framework for studying 2D quantum states, including systems with topological order and exotic phases of matter. These examples illustrate the versatility of TN representations in capturing the essential properties of quantum states. MPS and PEPS have proven to be invaluable tools for understanding and characterizing the behavior of 1D and 2D quantum systems, respectively. By utilizing TN diagrams, researchers gain insight into the entanglement structure and correlations within these states, facilitating further investigations and discoveries in the field of quantum physics.

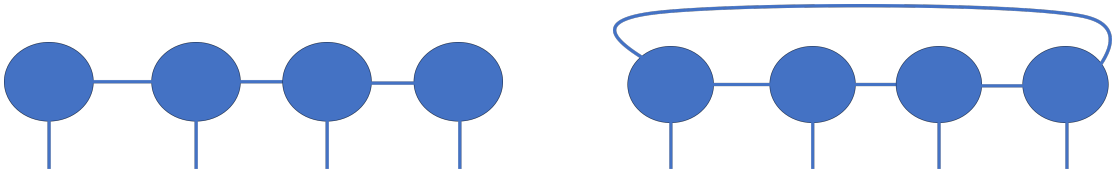

(a) (b)

Figure 2.3: (a) 4-site MPS with open boundary conditions; (b) 4-site MPS with periodic boundary conditions.

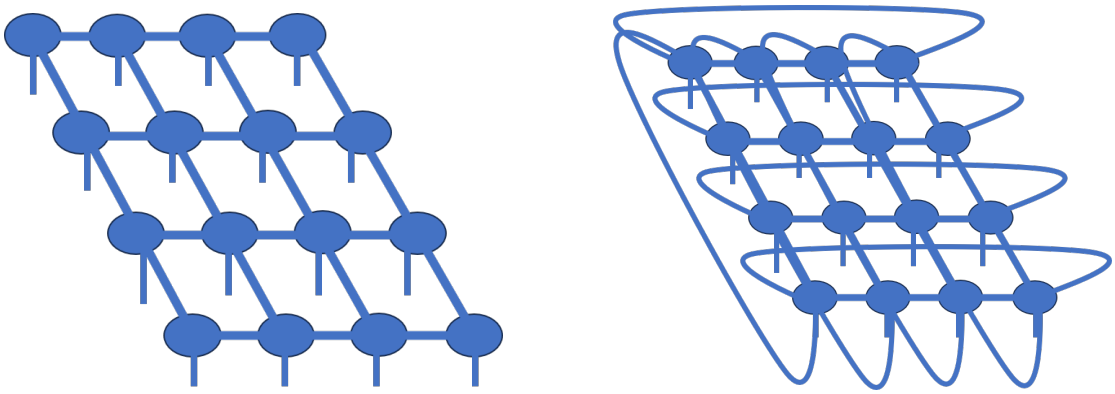

(a) (b)

Figure 2.4: 4×4 PEPS: (a) open boundary conditions, and (b) periodic boundary conditions.

2.3 Arbitrary quantum state to MPS

To convert an arbitrary quantum state into an MPS, Singular Value Decomposition (SVD) can be employed. The SVD allows us to express a matrix as a sum of products of orthogonal vectors and singular values. In the context of MPS, the state matrix is decomposed into a product of tensors. By absorbing the singular

values into the tensors, we can obtain different Canonical Forms for the MPS. Here, we'll describe three common forms:

1. Left Canonical Form: In this form, the singular values are absorbed into the tensor on right side as shown in Fig. 2.5.

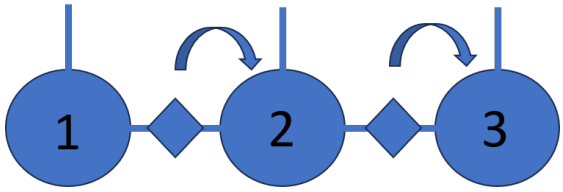

Figure 2.5: Left Canonical Form.

2. Right Canonical Form: In this form, the singular values are absorbed into the tensor on left side as shown in Fig. 2.6.

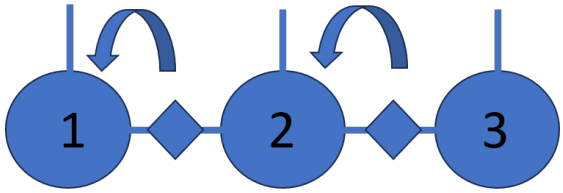

Figure 2.6: Right Canonical Form.

3. Mixed Canonical Form: In this form, the singular values are distributed between the left and right tensors. In this form, the left tensor absorbs the singular values that are to the left of a specified tensor while the right tensor absorbs the singular value that is to the right of specified tensor as shown in Fig. 2.7.

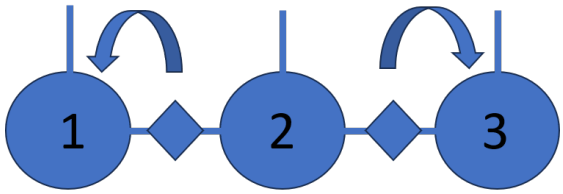

Figure 2.7: Mixed Canonical around site 2 (DMRG form).

2.4 Tensor Network Operators

Just as a state can be decomposed into a TN state (e.g., MPS, PEPS, etc.), an operator that acts on that state can also be decomposed into a similar TN operator. Below, we describe such an operator for MPS and its operation on an MPS.

2.4.1 Matrix Product Operator

A Matrix Product Operator (MPO) is an operator expressed in the matrix product form, similar to the MPS representation of quantum states. While an MPS represents a quantum state, an MPO represents an operator that acts on quantum states as shown in Fig. 2.8.

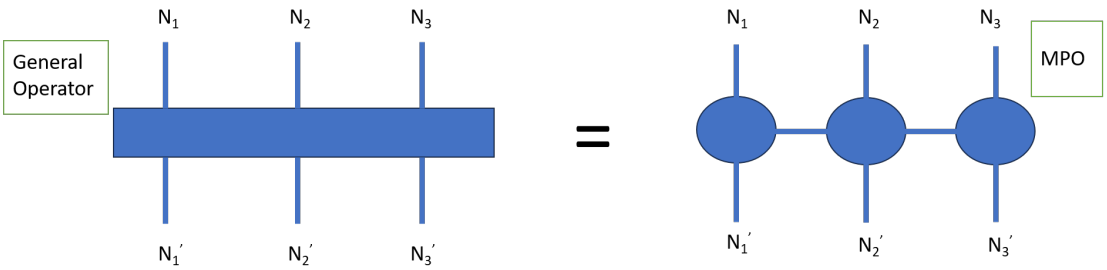

Figure 2.8: Conversion of a general operator to MPO.

An MPO consists of a set of matrices, each associated with a specific site or degree of freedom in the quantum system. These matrices capture the local interactions and transformations imposed by the operator. The MPO matrices are arranged in a one-dimensional chain, just like in an MPS, and they can be contracted with the corresponding MPS matrices to calculate the action of the operator on the state. Mathematically an MPO may be written as:

$$O^{n_1 n_2 n_3 \ldots n_l}_{n_1' n_2' n_3' \ldots n_l'} = \sum_i W^{n_1, n_1'}_{i_1} W^{n_2, n_2'}_{i_1 i_2} W^{n_3 n_3'}_{i_2 i_3} \ldots W^{n_l n_l'}_{i_l}. \tag{2.2}$$

where $W^{n_z, n_z'}_{i_x i_y}$ represent matrices for each site.

2.4.2 MPO Acting on MPS

When an MPO acts on an MPS, it represents the action of an operator on a quantum state. This is analogous to the Schrödinger equation where the Hamiltonian operator acts on a wavefunction. The result of applying the MPO to the MPS is a new MPS.

In the context of MPS, the bond dimension represents the number of entangled degrees of freedom between adjacent sites. Let's consider an MPS with a bond dimension of M_1 and an MPO with a bond dimension of M_2. When the MPO acts on the MPS, the resulting MPS will have a bond dimension of M_1 x M_2 as shown in Fig. 2.9. This means that the entanglement within the MPS has increased as a result of the action of the MPO.

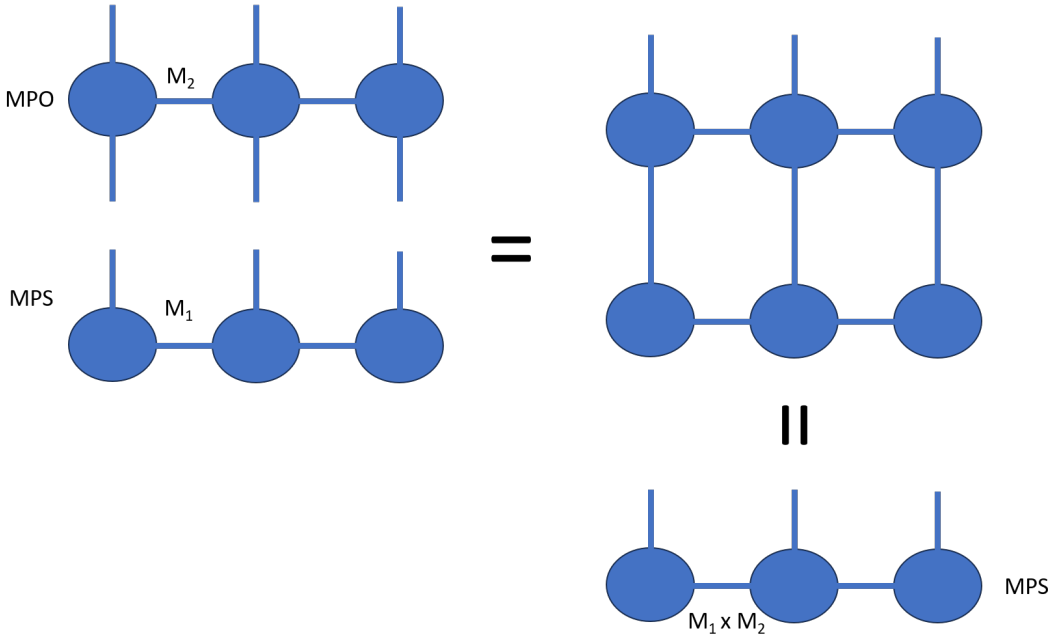

Figure 2.9: An MPO acting on MPS resulting in a new MPS.

In practical calculations, it is important to control and truncate the growth of entanglement. The exponential growth of the bond dimension can quickly become computationally intractable, especially for large systems. To address this, various truncation techniques are employed to limit the bond dimension of the resulting MPS. One common approach is to perform a SVD and retain only the largest singular values, discarding the smaller ones. This truncation helps to approximate the resulting MPS with a lower bond dimension, thereby reducing the computational complexity while still capturing the essential physics of the system.

2.5 Compression algorithms

2.5.1 MPS Compression: SVD

One approach to controlling and truncating the entanglement growth when applying an MPO to an MPS is through MPS compression using SVD. This method involves transforming the MPS into the Vidal Gauge, where the bond dimensions are reduced by keeping only the most significant singular values. By doing so, an efficient low-rank approximation of the MPS is obtained. However, this technique compresses each site independently, without considering the influence of neighboring states. This local update approach may result in the loss of critical information, limiting its effectiveness.

2.5.2 MPS: Variational Compression

A more robust approach to compression is to treat it as an optimization problem. By formulating a minimization problem, the goal is to find the compressed state that minimizes the difference between the new compressed state and the original state. This can be achieved by iteratively following the gradient until it vanishes. The optimization process involves differentiating the minimization expression with respect to the elements of the matrix, enabling the computation of the gradient. Notably, this variational compression technique takes into account information discarded in each truncation when truncating the next bonds. It provides a more comprehensive approach compared to independent local updates, as the optimization for each site depends on all other sites, utilizing the full environment.

2.5.3 Sweep Algorithm (DMRG Style)

The Density Matrix Renormalization Group (DMRG) algorithm employs a sweep algorithm to address the entanglement growth and control truncation. DMRG recognizes that explicitly following the gradient is not necessary when working in the mixed canonical form. It leverages the linear nature of operations in the matrix product state, reducing the problem to linear algebra operations. The minimization is performed site by site, solving linear equations for each site. In each iteration, the updated site is used to update the neighboring sites, ensuring the entanglement is controlled and truncated effectively.

These algorithms provide different strategies for controlling the entanglement growth when applying a MPO to an MPS. While MPS compression via SVD offers a simple approach, variational compression and sweep algorithms, such as the one used in DMRG, provide more robust and optimized methods for truncating and controlling the entanglement while preserving critical information in the system. The choice of algorithm depends on the specific requirements and characteristics of the quantum system being studied.

2.6 Energy optimization

In DMRG energy minimization, the goal is to find the optimal tensor for each site of the MPS by solving an eigenvalue problem. Under the hood, DMRG combines a variational approach with the concept of a finite-size environment. The DMRG algorithm starts with an initial guess for the MPS and constructs the effective Hamiltonian for a block of neighboring sites. The effective Hamiltonian captures the low-energy physics of the system within the block by taking into

account the entanglement between the block and its surrounding environment. Next, DMRG performs a diagonalization of the effective Hamiltonian to obtain the ground state and its corresponding eigenvalues. This is done by iteratively updating the MPS tensors for each site, optimizing them to minimize the energy. The optimization process typically involves using iterative methods such as the Lanczos algorithm [18] or the Davidson algorithm [19]. During each iteration, a sweep is performed through the lattice, optimizing one site at a time. At each site, the tensor is updated by diagonalizing the local Hamiltonian and selecting the eigenvector corresponding to the lowest eigenvalue. This eigenvector becomes the new tensor, and the process is repeated for the next site. The crucial aspect of DMRG is the use of a finite-size environment to capture the long-range entanglement in the system. By gradually increasing the size of the block, DMRG incorporates more of the environment's influence, improving the accuracy of the ground state approximation. The DMRG algorithm continues iterating through the lattice, sweeping back and forth, until convergence is reached and the energy is minimized. The resulting MPS represents an approximate ground state of the system. DMRG energy minimization is computationally expensive due to the need to solve the eigenvalue problem for each site and the full environment calculation. However, it is known for its high accuracy in obtaining ground state energies and has been successful in a wide range of condensed matter physics problems. In contrast, the Time-Evolving Block Decimation (TEBD) algorithm takes a different approach by performing local updates and imaginary time evolution combined with SVD compression. While TEBD is more computationally efficient, it may not capture long-range entanglement as effectively as DMRG, potentially leading to less accurate results in certain scenarios.

2.7 Time evolution

In general, time evolution involves applying a unitary operator to a given state to propagate it in time. Let's consider the time evolution of a MPS with respect to a Hamiltonian. For real-time evolution, the unitary operator can be expressed as e^{-iHt}, where H is the Hamiltonian of the system and t is the time parameter. Applying this unitary operator to the MPS results in a new MPS with a larger bond dimension, representing increased entanglement. To perform imaginary time evolution, the unitary operator is modified by replacing the imaginary unit "i" with the real number "1". The modified unitary operator can be expressed as U = e^{-Ht}. The effect of imaginary time evolution is to "cool" the system towards its ground state. By repeatedly applying imaginary time evolution, the state con-

verges towards the ground state of the Hamiltonian. In both cases, after applying the time evolution operator to the MPS, the resulting state may have a larger bond dimension, which represents increased entanglement. To control the growth of entanglement and keep the MPS in a manageable form, compression techniques such as SVD can be employed. Compression involves truncating the bond dimensions by keeping only the most significant singular values. This compression step helps maintain a compact representation of the state while controlling the entanglement growth. The process of time evolution in MPS typically involves repeated iterations of applying the time evolution operator, followed by compression to control the entanglement growth. By iteratively applying time evolution and compression, one can simulate the dynamics of quantum systems and study their behavior over time.

2.7.1 Trotter decomposition

In lattice problems with short-range Hamiltonians, a commonly used technique for time evolution is Trotter decomposition [20]. This decomposition allows for the time evolution of a short-range Hamiltonian to be performed on individual bonds or interactions in the system, rather than considering the entire system as a whole. In the context of MPS, the time evolution can be divided into even and odd bonds. This means that the time evolution is applied to the bonds connecting neighboring lattice sites alternately. For example, in one step, the time evolution is applied to even bonds (1-2, 3-4, etc.), and in the next step, it is applied to odd bonds (2-3, 4-5, etc.). This iterative approach of evolving even and odd bonds is known as the even-odd evaluation scheme. This scheme of alternating the time evolution on even and odd bonds is compatible with the compression algorithm, such as SVD, which is used in techniques like TEBD. The key idea is that the SVD compression can be performed independently on each bond after the time evolution of neighboring bonds. For example, if the time evolution is applied to bonds 1-2 and 3-4 while leaving bond 2-3 unchanged, the resulting MPS will have a larger bond dimension. However, the compression step can be done independently on bond 1-2 and bond 3-4 since no changes were made to bond 2-3. This allows for efficient compression, as the compression can be performed on each bond separately without considering the entire system. By combining the even-odd evaluation scheme with the compression algorithm, such as SVD, in techniques like TEBD, the time evolution of lattice systems with short-range Hamiltonians can be simulated efficiently. This approach allows for the controlled growth of entanglement and maintains a compact representation of the state during the time evolution process.

2.8 Periodic and infinite MPS

MPS can be readily extended to incorporate periodic boundary conditions (PBC) and describe systems in the thermodynamic limit. These extensions allow for the study of infinite systems and the simulation of long-range correlations. For systems with PBC, the MPS representation is modified to include the bonds connecting the first and last sites of the system. By explicitly considering these bonds, the MPS captures the periodicity of the system and allows for the calculation of physical properties and correlations across the entire system. In the thermodynamic limit, where the system size becomes infinitely large, MPS can be used to describe the properties of the system. In this case, the MPS tensors and bond dimensions are kept fixed, while the system size increases. By carefully considering the behavior of the MPS tensors and adjusting the bond dimensions, it is possible to accurately capture the properties of an infinite system using a finite set of tensors.

Local algorithms, such as Time-Evolving Block Decimation (TEBD), are well-suited for simulating infinite MPS. These algorithms operate on a local scale and can efficiently handle the propagation and compression of the MPS tensors, making them easily extendable to infinite MPS. By iteratively applying the time evolution operators on neighboring bonds and performing compression steps, local algorithms can simulate the dynamics and thermodynamic properties of infinite systems described by MPS. The ability to extend MPS to systems with PBC and in the thermodynamic limit greatly enhances the applicability of these techniques, allowing for the study of a wide range of physical phenomena in condensed matter physics and quantum many-body systems.

2.9 Symmetries

In MPS, symmetries play a crucial role in understanding and characterizing the properties of quantum systems. Symmetries are associated with both the physical indices (site basis) and the bond indices in MPS. For global symmetries, such as U(1) particle number symmetry [21] or SU(2) angular momentum symmetry [22], the site basis of the Hamiltonian are labeled by irreducible representations of the corresponding symmetry group. In the case of U(1) symmetry, the site basis are labeled by an integer quantum number representing the particle number, while for SU(2) symmetry, the site basis are labeled by the total angular momentum and its projection along a chosen axis. By exploiting these symmetries, the total state of the system is written in terms of these good quantum numbers associated with the symmetries. This simplifies the representation of the state and allow for more

efficient calculations, as only states with compatible quantum numbers need to be considered. Importantly, the bond indices in MPS also inherits symmetries from the physical indices. For example, if there is a U(1) symmetry associated with the physical indices, it implies that the bond indices will also have an effective particle number symmetry. Similarly, if there is an SU(2) symmetry, there will be an angular momentum quantum number symmetry on the bond indices. This means that the bond indices can be labeled by the same symmetry labels as the physical indices. In addition to these symmetries associated with the physical and bond indices, MPS may also possess topological quantum numbers. These topological quantum numbers are associated with the higher-dimensional bond indices and represent nontrivial topological properties of the system. These topological quantum numbers may be used to classify and distinguish different phases of matter.

Chapter 3

Tensor Network Renormalization

In the study of emergent phenomena in many-body systems, the goal is to understand how individual particles or constituents collectively organize themselves to give rise to macroscopic behavior such as metal, insulator or phenomena as superconductivity, super-fluidity, etc. The challenge lies in deriving these collective behaviors from the microscopic interactions between the particles or atoms. One approach to tackle this problem is through the combination of renormalization group (RG) techniques and tensor networks, leading to the development of the Tensor Network Renormalization (TNR) method. TNR aims to capture the essential features of the many-body system and extract emergent properties from the microscopic interactions.

3.1 RG applied to Quantum Ising Model

The use of tensor networks, such as the TNR method, allows for the efficient representation and manipulation of partition functions and path integrals. Tensor network techniques provide a framework for approximating and analyzing the properties of many-body systems by capturing the relevant information while reducing the computational complexity. By combining renormalization group ideas with tensor network methods, researchers can gain insights into the collective behavior and emergent phenomena in many-body systems. The TNR approach, in particular, offers a powerful tool for studying quantum models and extracting valuable information about phase transitions, critical phenomena, and the behavior of quantum states in various dimensions. To illustrate this, let's consider the example of the quantum Ising model, specifically a one-dimensional spin chain where σ^z and σ^x represent the z and x pauli matrices respectively, J represents the strength of the coupling between neighboring spins and λ represents the strength of the

transverse magnetic field.

$$H_q^{1d} = J \sum_i \sigma_i^x \sigma_j^x + \lambda \sum_i \sigma_i^z \tag{3.1}$$

The idea of the RG is to study how these couplings evolve as we change the scale of observation. When we zoom out and look at the system from a bigger scale, we discover that the behavior of the system at that scale may be described by an effective Hamiltonian. The couplings in the Hamiltonian may change as we move to larger or smaller scales, leading to a flow in the space of couplings or Hamiltonians. In the RG picture, we consider a space of couplings or Hamiltonians, and we identify distinct regions or phases within this space. For example, in the Ising model, we may have a green region and a blue region. We observe a non-trivial flow in this space, where starting from a particular Hamiltonian, it will flow towards a fixed point as we change the scale.

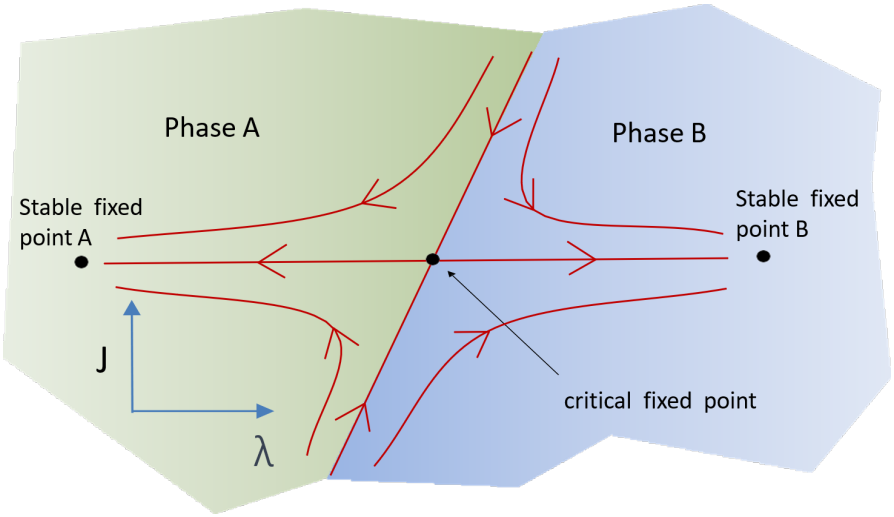

Figure 3.1: RG flow in space of Hamiltonian. [23]

The flow in the space of couplings or Hamiltonians can divide the space into different phases. In the Ising model, we may have stable fixed points corresponding to different phases. If we start from the green region, the flow will take us to one stable fixed point, while starting from the blue region will lead us to another stable fixed point as shown in Fig. 3.1. In between these phases, we may have a critical fixed point, corresponding to the phase transition.

3.2 Elimination of Short Range Interactions

The RG provides a powerful framework for understanding the behavior of physical systems and identifying different phases, phase transitions, and the emergence of

critical phenomena. By studying the flow of couplings or Hamiltonians under the RG transformation, we can gain insights into the collective behavior of many-body systems and their universal properties. In non-perturbative renormalization group approaches, the goal is to perform coarse-graining transformations in a universal and objective manner, applicable to a generic system. One key ingredient in these approaches is the removal of short-range interactions so that the physics of low scale could be separated from physics of high scale. One such approach that satisfies these requirements is the real-space RG method. In this method, the system is divided into blocks or cells, each containing multiple lattice sites or degrees of freedom. The RG transformation involves integrating out the degrees of freedom within each block to obtain an effective description of the system at a coarser scale.

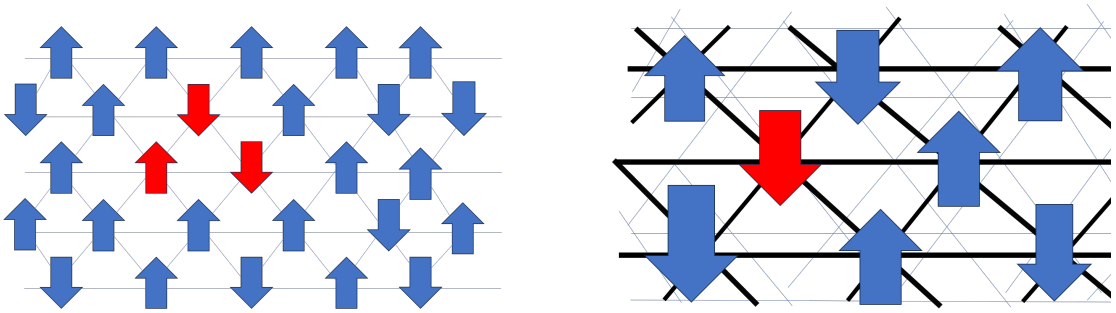

Figure 3.2: Coarse graining by majority vote of spins. To get an effective description at a higher scale, a spin is selected and depending upon where the majority of its immediate neighbours point at, it is denoted as spin up or spin down. This is then repeated for other spins.

The procedure can be summarized as follows: 1. Divide the system into blocks or cells, where each block contains multiple lattice sites or degrees of freedom. 2. Construct an effective Hamiltonian for each block by integrating out the degrees of freedom within the block. This involves taking the trace over the removed degrees of freedom and obtaining an effective coupling or interaction term for the block. 3. Combine the effective Hamiltonians of neighboring blocks to obtain the effective Hamiltonian at the next coarser scale as shown in Fig. 3.2. 4. Repeat steps 1-3 iteratively, treating the effective Hamiltonian at each scale as the new microscopic Hamiltonian for the next scale. 5. Analyze the flow of couplings or interactions under these coarse-graining transformations to identify fixed points and phases.

The key idea behind this approach is that by removing short-range interactions and integrating out degrees of freedom, we effectively capture the long-range or collective behavior of the system. The iterative nature of the RG transformation allows us to study the system at different scales and observe how the couplings or interactions evolve. By performing the coarse-graining transformations in a sys-

tematic and universal manner, non-perturbative RG approaches provide insights into the universal properties and behavior of diverse systems, regardless of their specific details. These methods have been successfully applied to a wide range of systems, including quantum spin systems [24], lattice models [25], and field theories [26], providing valuable insights into phase transitions, critical phenomena, and emergent phenomena in many-body systems.

3.3 MERA

MERA (Multi-scale Entanglement Renormalization Ansatz) is an efficient representation of many-body wavefunctions. It is depicted as a tensor network structure where each tensor represents a variational parameter. The MERA structure shown in Fig. 3.3 extends both in space and scale, allowing it to capture correlations at different length scales in the system.

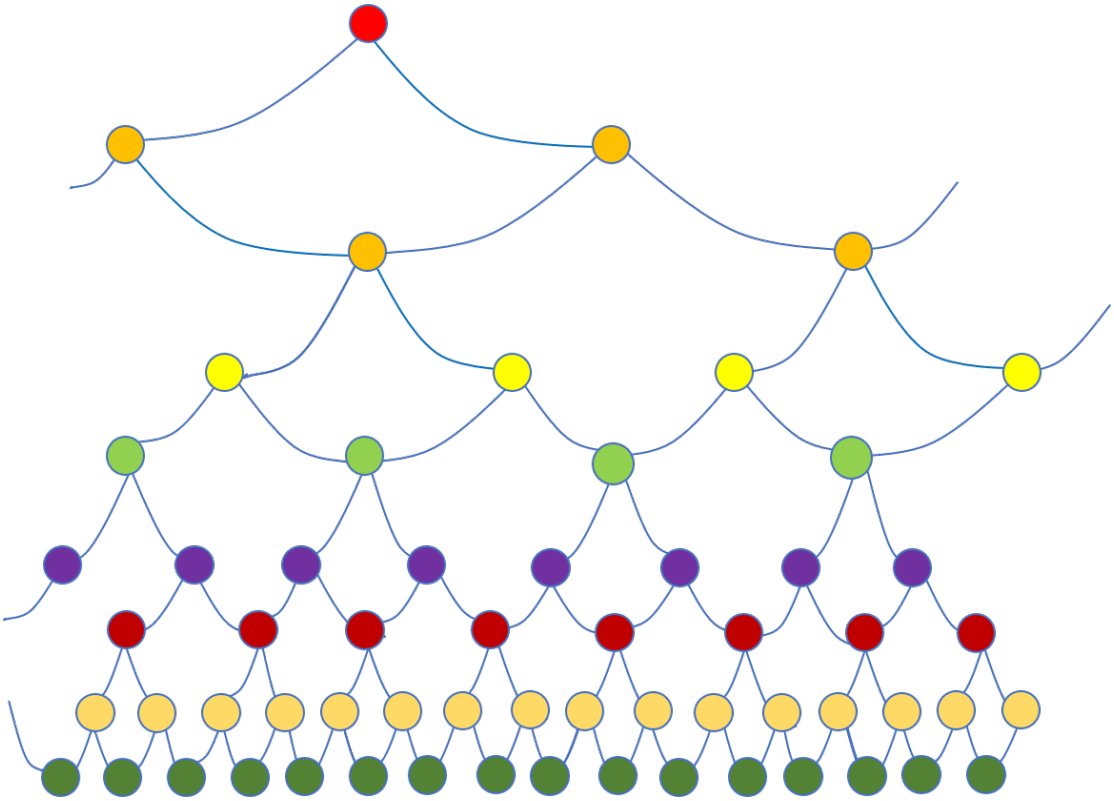

Figure 3.3: MERA (Multi-scale Entanglement Renormalization Ansatz. MERA presents a hierarchical network of tensors arranged in a tree-like structure. It is designed to capture the entanglement structure of the quantum state, emphasizing the crucial long-range entanglement present in critical systems.)

MERA can be viewed as both a quantum circuit [27] and a renormalization group transformation [28]. As a quantum circuit, it uses disentanglers [29] and isometries [30], which are two-body gates, to introduce entanglement into the

wavefunction at different scales. This enables the representation of ground states with correlations at all length scales, as expected in quantum critical systems. On the other hand, MERA can also be understood as an RG transformation. It performs a coarse-graining procedure where it groups sites together and updates the variational parameters to capture the effective properties of the system at a coarser scale. This transformation allows the MERA to capture the universal features of the system and provides insights into the emergent phenomena and phase transitions. MERA combines the concepts of quantum circuits and RG transformations to efficiently represent many-body wavefunctions and study their properties.

3.3.1 MERA as RG Transformation

In the context of studying complex systems, such as those in condensed matter physics, the RG transformation provides a powerful framework for understanding their behavior at different length scales. The primary goal of the RG transformation is to simplify the system by reducing its degrees of freedom while preserving its essential properties. In the context of the renormalization group transformation, the blocking strategy proposed by Leo Kadanoff [31] involves grouping spins on a lattice to obtain an effective lattice with fewer spins. This coarse-graining procedure reduces the degrees of freedom and allows for the study of the system at larger length scales. Steve White's Density Matrix Renormalization Group (DMRG) method builds upon this idea by introducing variational energy minimization to determine the optimal blocking transformation [32]. In the modified version of the coarse-graining transformation used in MERA, additional elements are introduced. In addition to combining two spins into one effective spin, the transformation includes disentanglers and isometries. The disentanglers are unitary transformations applied to a spin and its neighboring spin to reduce the entanglement between them. The isometries represent the grouping of spins into an effective spin after the disentanglement process. MERA framework extends and modifies the original blocking transformation proposed by Kadanoff, incorporating variational energy minimization, disentanglers, and isometries. This combination allows for an efficient representation of many-body wavefunctions and the study of emergent phenomena in quantum systems. In the blocking scheme used in MERA, the presence of entanglement between neighboring sites that are going to become the same site in the coarse-grained description can lead to the propagation of short-range entanglement into long-range entanglement. This is undesirable because it introduces unnecessary details at longer length scales instead of removing them, which goes against the goal of a proper renormalization group transformation as

shown in Fig. 3.4.

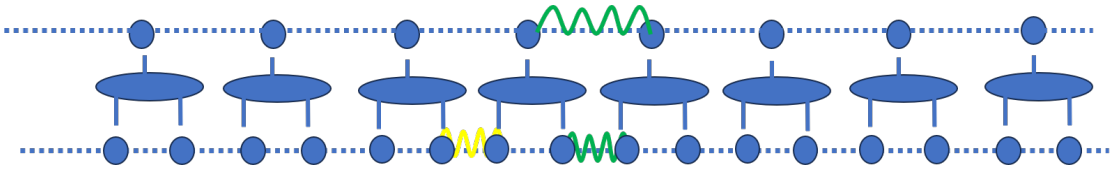

Figure 3.4: RG Transformation obtained by Kandoff's blocking scheme [33] and White's Variational optimization [32] fails to remove some short-range entanglement shown here as a green squiggle whereas the entanglement shown in yellow squiggle is removed.

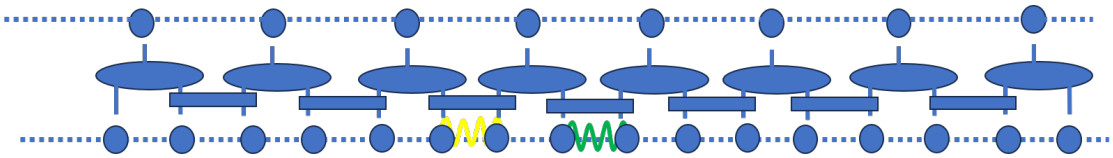

Figure 3.5: Entanglement Renormalization scheme [34] ensures removal of short-range entanglement by usage of disentanglers as shown where both yellow and green squiggles displaying entanglement are removed.

To address this issue, MERA introduces extra tensors called disentanglers. These disentanglers are applied before the spin blocking process, effectively disentangling the entangled spins. By removing the short-range entanglement before the spin blocking, MERA ensures that only the universal features and longer-range correlations are retained in the coarse-grained description as shown in Fig. 3.5. This allows for a more effective removal of short-range details and a focus on the essential aspects of the system's behavior at larger scales. The inclusion of disentanglers in MERA plays a crucial role in achieving the desired renormalization group transformation, where short-range entanglement is effectively removed from the system. By controlling and managing the entanglement structure at each step of the transformation, MERA provides a more objective and universal way of coarse-graining, leading to an efficient representation of many-body wavefunctions and capturing the essential features of the quantum system. In MERA, the wave functions at different length scales form a collection or network of wave functions, which describe a flow in the space of wave functions. By removing a layer of coarse graining in the MERA tensor network, we obtain an effective wave function at a different length scale. By repeating this process and removing additional layers, we can obtain wave functions corresponding to different length scales. Although the initial objective was to establish a renormalization group flow within the domain of Hamiltonians, the MERA construction offers a renormalization group flow within the realm of wave functions. However, this is still beneficial because we can use the MERA framework to define a coarse graining transformation for the Hamiltonian

Table 3.1: Comparison of Exact Scaling Dimension and Scaling Dimension achieved by MERA. [33]

	Exact Scaling Dimension	**Scaling Dimension (MERA)**	**Error**
Identity	0	0	—
Spin	0.125	0.124997	0.003%
Energy density	1	0.99993	0.007%
Disorder	0.125	0.1250002	0.0002%

as well. By applying the same coarse graining transformation to the Hamiltonian, we obtain an effective Hamiltonian at a different length scale, allowing us to define an energy flow in the space of Hamiltonians. In this way, MERA provides a unified approach where both the wave functions and the Hamiltonians undergo a renormalization group flow. This allows for the study of emergent phenomena and the exploration of the energy landscape in the space of Hamiltonians using the MERA framework. In practice, when applying the MERA ansatz to the critical Ising model, we can extract valuable information and achieve high accuracy in the results. By optimizing the ansatz through energy minimization, we obtain the scaling dimensions of primary fields in the Ising conformal field theory (CFT) [35]. The obtained scaling dimensions are consistent with the exact solutions, with high accuracy reaching several digits as shown in Table: 3.1. This accuracy extends to the study of non-local primary fields, fermions, and other operators.

The MERA ansatz allows us to extract various conformal data, including the central charge, scaling dimensions, conformal spin, and operator product expansion coefficients. By exploiting translation invariance and scaling variance, we can study infinite systems using a compact representation, specifying a unit cell of tensors that repeats through space and scale, effectively capturing the thermodynamic limit.

3.3.2 MERA and Holography

The connection between MERA and holography [36] has also been explored. The MERA tensor network exhibits logarithmic scaling of entanglement entropy for critical systems in one spatial dimension, resembling the behavior seen in holographic theories. The calculation of entanglement entropy in MERA parallels the concept of minimal surfaces in the Ryu-Takayanagi formula [37]. Additionally, two-point correlators in MERA decay exponentially with distance, following a power-law behavior. This correspondence with holography has led to the proposition that MERA could serve as a toy model for understanding aspects of quantum gravity and holography [38]. The exploration of MERA's connection to holography

and its potential implications for understanding quantum gravity has attracted interest and contributions from researchers in the field. While more investigation is needed, there is promising evidence that MERA could provide valuable insights into quantum gravity at some level.

Chapter 4

Simulation of quantum light using MPS

4.1 Investigating strong interactions and many-body phenomena in photon-atom ensembles: A novel numerical approach

Transmission of light through an atomic ensemble is a key approach for establishing a connection between quantum phenomena related to light and matter. Recently, Rydberg ensembles have emerged as a prominent system for achieving strong interactions between photons that exhibit non-linearity [39]. However, it is uncertain whether these systems can generate distinct many-body states of light, as shown in Fig. 4.1, which necessitates the development of new techniques to investigate scenarios involving a large number of photons. One such approach is the utilization of a spin model method that maps the dynamics of one-dimensional light propagation onto an open, interacting spin system. By analyzing the correlations among the spins, it becomes possible to infer correlations among photons. This framework allows for the exploration of phenomena like vacuum-induced transparency, where pulse components with varying photon numbers propagate at different velocities leading to their separation at the output. By employing matrix product states, the spin dynamics can be effectively solved through numerical methods. This approach facilitates the examination of the interplay between light and atomic ensembles, thereby driving progress in the field of quantum technologies.

In general, the presence of weak optical nonlinearities in atomic ensembles imposes limitations on processes that can be adequately described using classical

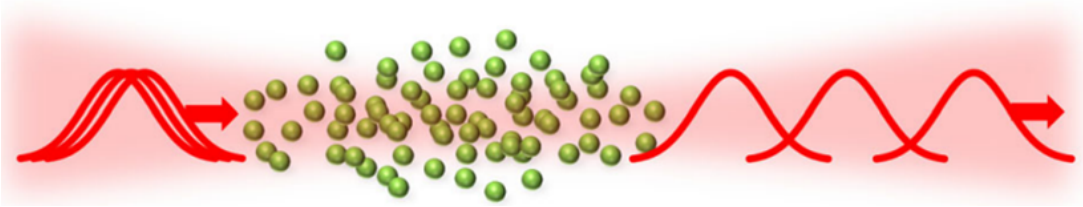

Figure 4.1: The influence of strong inter-atomic interactions on quantum light properties: crystalline-like photon emission from atomic ensembles [1].

linear optics or Gaussian quantum states [40]. However, recent progress has made it possible to achieve strong interactions among photons within atomic ensembles, leading to the emergence of highly non-Gaussian states [41]. Experimental demonstrations of phenomena like photon blockade [42] or two-photon bound states [43] have been achieved with weak field inputs in atomic Rydberg gases. Other systems, such as photonic waveguides coupled to atoms or "artificial" atoms like superconducting qubits [44] and quantum dots [45], hold promise for achieving similar outcomes. Exploring strong interactions between photons in atomic ensembles with higher field inputs is expected to reveal intriguing many-body phenomena, including photon crystallization. However, addressing this question theoretically poses challenges due to the system's out-of-equilibrium nature, openness, and long-range interactions between atoms facilitated by photon exchange. Although certain progress has been achieved in specific regimes [46] [47], the effectiveness of theories derived from certain approximations is limited in its applicability. Consequently, there exists a pressing need to develop numerical methods that minimize approximations, allowing for the validation of these models and the exploration of regimes where the approximations become invalid.

Currently, numerical techniques face constraints, and the standard approach involves using Maxwell-Bloch equations to describe the dynamics of atom-light interactions. The solution to these equations involves discretizing the atomic and photonic fields, as illustrated in Fig. 4.2. However, this approach limits numerical simulations to systems with two or three total excitations and overlooks the complete effects of dissipation. In summary, we discuss a novel numerical method for simulating light propagation in atomic ensembles, which enables the study of many-body phenomena involving photons in regimes of strong interactions, such as photon crystallization [48]. The approach utilized in this method entails representing the problem through the dynamics of a one-dimensional open spin model. This model can be effectively addressed by applying the MPS ansatz derived from condensed matter physics. This technique is well-suited for treating chains of hundreds of spins, and we provide heuristic arguments to support its applicability to atom-light interfaces. To validate their model, we employ it to simulate pulse

propagation in the context of vacuum-induced transparency, one of the few cases where there is a qualitative understanding of many-photon propagation.

Figure 4.2: Numerical treatment of quantum light propagation: Discrete space division and Fock basis states. In the conventional numerical approach for modeling quantum light propagation, the spatial domain is divided into M discrete units centered at positions z_j, each associated with local Fock basis states $|0\rangle$, $|1\rangle$. Within this discretized spatial framework, it becomes possible to solve the equations of motion governing the field [1].

4.2 1D spin model of light propagation

A different approach for describing the interaction between light and matter in a quasi-one-dimensional system involves modeling the system as a 1D waveguide coupled to a collection of N atoms. By integrating out the degrees of freedom related to the light field in this simplified representation, an effective model emerges. This model comprises an interacting "spin" chain, where each spin corresponds to an internal state of an atom. The output field can be computed directly from the dynamics of the spins using an input-output relation [49]. As a result, the Hilbert space is reduced to the atomic degrees of freedom, which can be effectively handled using matrix product states, ensuring computational efficiency.

The coupling between the atoms and the waveguide modes is characterized by a strength denoted as Γ_{1D}. In the case of two-level atoms, the excited state $|e\rangle$ can also decay into modes outside of the waveguide, with a decay rate represented by Γ'. The electric field operator can be expressed as the sum of a forward propagating mode, denoted as $E_+(z,t)$, and a backward propagating mode, denoted as $E_-(z,t)$. These modes are governed by propagation equation:

$$\left(\frac{1}{c}\frac{\partial}{\partial t} \pm \frac{\partial}{\partial z}\right) E_\pm(z,t) = i\sqrt{\frac{\Gamma_{1D}}{2}} P_{ge}(z,t). \tag{4.1}$$

This propagation equation, commonly referred to as the one-dimensional, paraxial Maxwell-Bloch equation, is governed by the atomic polarization density operator

$P_{\mathrm{ge}}(z)$. This operator describes the interaction between the atoms and the electromagnetic field and follows an optical Bloch equation [50]:

$$\frac{\partial P_{\mathrm{ge}}(z,t)}{\partial t} = -i\left(\omega_{\mathrm{eg}} - \frac{i\Gamma'}{2}\right) P_{\mathrm{ge}}(z,t) + i\sqrt{\frac{\Gamma_{1D}}{2}}\left[P_{\mathrm{gg}}(z,t) - P_{\mathrm{ee}}(z,t)\right] E(z,t) + F(t). \tag{4.2}$$

where ω_{eg} is the atomic transition frequency, P_{gg} is the ground state population and P_{ee} is the excited state population. By integrating the equations, it is possible to obtain a solution for the field. This solution comprises the sum of the input field $\mathcal{E}_{\mathrm{in}}$ and the field radiated by the atoms within the waveguide.

$$E\left(z,t\right) = \mathcal{E}_{\mathrm{in}}\left(z,t\right) + i\sqrt{\frac{\Gamma_{\mathrm{1D}}}{2}} \sum_{i=1}^{N} e^{ik_0|z-z_i|}\sigma_{\mathrm{ge}}^{i}(t). \tag{4.3}$$

where k_0 is a wavevector given by ω_{eg}/c and $\sigma_{\mathrm{ge}}^{i}(t)$ is the local spin operator for i-th atom. This simplified model provides a convenient framework for analyzing and understanding the behavior of the system. It can be used to explore the effects of different parameters and conditions on the system, and to develop new strategies for controlling the interaction between light and matter.

In order to accurately replicate phenomena observed in atomic ensembles in free space, it is crucial to make deliberate choices regarding the coupling of atoms to the waveguide and the positions of the atoms. These choices need to be made carefully to ensure accurate representation and alignment with the observed phenomena. Numerical calculations are facilitated by selecting appropriate ratios between the 1D coupling strength Γ_{1D} and the scattering rate Γ'. The transmittance T, defined as the ratio of the output field intensity to the input field intensity, can be expressed as $T = \exp(-\mathrm{OD})$, where OD represents the optical depth. The optical depth is proportional to the number of atoms N and the 1D decay rate Γ_{1D}, while inversely proportional to the scattering rate Γ'. By selecting suitable values such as $\Gamma_{\mathrm{1D}} \lesssim \Gamma'$ and a waveguide spacing of $k_0 a = \frac{\pi}{2}$ where a is the spin chain lattice constant, it is possible to achieve the same optical depth as realistic atomic ensembles with just tens or hundreds of atoms. Most quantum nonlinear optical phenomena are believed to depend primarily on the optical depth or a limited number of other parameters, where the atom number does not independently appear.By precisely matching these parameters using a smaller number of atoms, it becomes feasible to effectively model the desired physics in three-dimensional atomic ensembles. To ensure the elimination of potential artificial effects arising from low atom numbers, it is important to numerically verify the convergence of observables with increasing N while adjusting Γ_{1D} proportionally to maintain the key parameters constant.

4.3 Simulations using Matrix Product States

The use of MPS provides a practical and efficient approach for simulating light propagation in atomic ensembles, especially when the Hilbert space dimension becomes large. Through the truncation of the Hilbert space and the implementation of MPS, it becomes possible to represent the quantum state of the spin chain using a localized description. This approach retains only a manageable number of basis states, making it computationally feasible to handle and analyze the system efficiently. These basis states are dynamically updated during time evolution to optimize their overlap with the actual state wave function.

For systems with short-range interactions typically observed in atomic ensembles, MPS have been shown to be efficient [51]. The scaling behavior of the bond dimension (D) in MPS is reasonable in the absence of additional interactions beyond the dipole-dipole interaction. Despite possessing an infinite-range and non-uniform nature, the dipole-dipole interaction maintains the conservation of excitation number. Consequently, it enables pulse propagation without causing significant entanglement generation. Moreover, experiments have demonstrated that the nonlinearity resulting solely from atomic saturation remains minimal at the single-photon level.

However, when additional interactions are present, the scaling of the bond dimension depends on the specific system and interactions involved. Under continuous driving scenarios, the system typically settles into a steady state within a memory time approximately equal to the pulse propagation time through the length of the system. This phenomenon helps restrict the growth of entanglement, ensuring a more stable and manageable quantum state. In the case of pulsed input, the number of photons in the pulse sets an upper bound on the entanglement, and the required bond dimension can be determined. While the scaling bound for arbitrary n-photon wave functions may still exhibit exponential growth, being on the order of $N^{(n/2)}$, certain benchmark cases like vacuum-induced transparency display a more favorable scaling behavior, approximately quadratic in the number of photons [52].

In the numerical simulation of the spin model using MPS and the quantum jump approach, several key manipulations of the MPS are performed to capture the time dynamics of the master equation. The steps involved are as follows:

1. Deterministic Evolution: The first step involves the deterministic evolution of the MPS representation of the state. A small discrete time step (δt) is chosen, and the time evolution operator ($e^{-iH_{\text{eff}}\delta t}$) is approximated and expressed as an MPO. The MPO captures the evolution under the effective Hamiltonian (H_{eff}) of

the system. This MPO is then applied to the MPS state representation, updating it to the new time step.

2. Stochastic Quantum Jumps: After the deterministic evolution, stochastic quantum jumps are applied to account for dissipation in the system. The quantum jump operators (O_l) are represented as MPOs, and these MPOs are applied to the MPS state representation. Each quantum jump increases the bond dimension, denoted as D_W, as new virtual indices are added to accommodate the additional degrees of freedom.

3. Compression: To control the growth of the MPS representation over time and keep the computational resources manageable, the state undergoes a compression step. This step reduces the bond dimension of the MPS, ensuring that it remains within a desired limit. Various compression techniques, such as singular value decomposition (SVD), can be employed to truncate the least significant contributions and retain the most important information.

4. Calculation of Observables: At each time step, observables of interest are calculated using the MPS representation and the corresponding MPO for the observable. This allows the evaluation of physical quantities and the analysis of the system's behavior during the simulation.

By repeating these four steps iteratively, the full time evolution of the system is obtained in the numerical simulation. The deterministic evolution captures the unitary dynamics, while the stochastic quantum jumps account for dissipation. The compression step helps manage the computational resources, and the calculation of observables provides insights into the physical quantities of interest.

4.4 Vacuum Induced Transparency

To benchmark the capabilities of MPS approach, we apply it on vacuum-induced transperancy (VIT). VIT is closely related to electromagnetically induced transparency (EIT), a phenomenon that occurs in three-level atomic media, as shown in Fig. 4.3. In VIT, the control field used in EIT is substituted with strong coupling between the atoms and a resonant cavity mode.

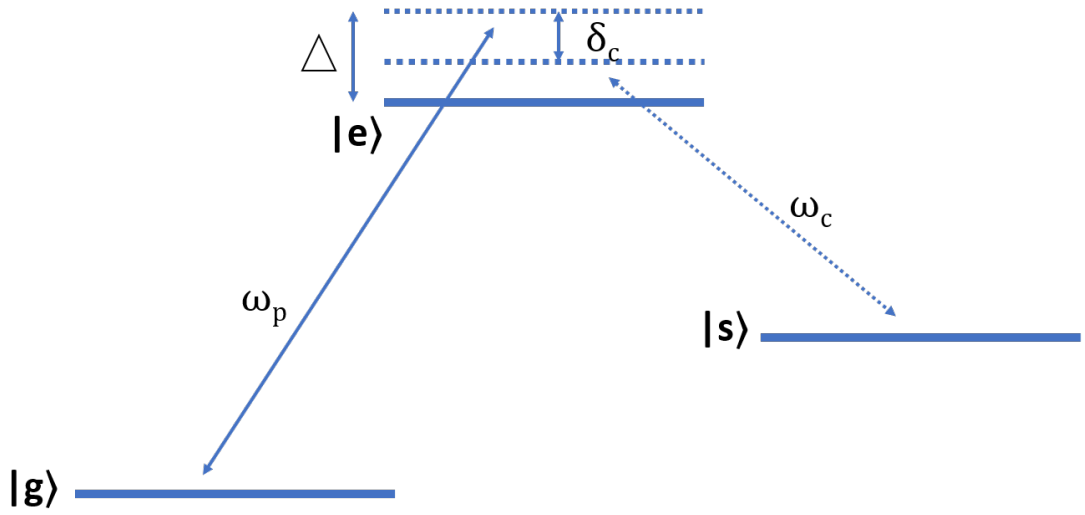

Figure 4.3: EIT setup where transparent propagation of probe photons ω_p can be achieved by coupling the transition $|s\rangle$-$|e\rangle$ of three-level atoms to a control or cavity field with frequency ω_c.

The coupling between the cavity mode and the atoms in VIT is described by the Hamiltonian

$$H_{cav} = g \sum_{j=1}^{N} (\sigma_{\text{es}}^{j} b + \text{H.c.})/2. \tag{4.4}$$

where g represents the uniform coupling among the atoms and the cavity mode, b represents the annihilation operator for cavity mode and σ_{es}^{j} represents the atomic operators for the excited and metastable states of the j-th atom. Even in the absence of any cavity mode occupation, the atomic medium can exhibit transparency through vacuum Rabi oscillations. These oscillations facilitate the transfer of population from the excited state $|e\rangle$ to the spin state $|s\rangle$ which causes nonlinear coupling between the atoms and the cavity, affecting the propagation of light in the system.

In VIT, the spin wave formation lead by n probe photons is accompanied by equivalent excitation of cavity photons. Resultantly, we get an effective control field strength of $\sqrt{ng}$, where n represents the number of photons and a number dependent group velocity $v_n \propto \frac{ng^2a}{2\Gamma_{1D}}$ [53, 54], where a is the lattice constant of the spin chain and Γ_{1D} is the decay rate of the excited state. This is in contrast with EIT, where the group velocity of light is dependent on the control field strength Ω ($v_g \propto \Omega^2$).

Fock states $|n\rangle$, which represent states with a fixed number of photons, are predicted to travel through the VIT system at speeds v_n based on the number of photons. On the other hand, given enough optical depth, it is expected that a coherent state $|\alpha\rangle$, which is a superposition of Fock states with an average

number of photons $|\alpha|^2$, will display spatial separation of its components due to their various propagation velocities. By adding a time delay to the input Fock components, $\tau_n = \frac{L}{v_n}$, where L is the length of the atomic medium, one may determine the output intensity.

By studying the dynamics of VIT and comparing the simulation results with the expected behavior described above, the simulation method is validated, and its effectiveness is demonstrated. Although exact solutions for complex multiphoton behavior are generally unavailable, understanding the qualitative nature of the system dynamics in the case of VIT provides valuable insights and serves as a benchmark for the simulation approach.

4.5 Methods

4.5.1 Quantum Jump Formalism

To investigate the temporal dynamics of the proposed model, time evolution of master equation must be performed. Numerical techniques like the Runge-Kutta algorithm enable us to directly evolve the complete density matrix ρ. An alternative method is the quantum jump approach, where the master equation is unraveled into evolving trajectories of pure states. In this method, MPS are employed, as explained below.

For our 1D spin model the master equation is expressed as follows:

$$\dot{\rho} = -i\left(H_{\text{eff}}\rho - \rho H_{\text{eff}}^{\dagger}\right) + \sum_{l} O_l \rho O_l^{\dagger}. \tag{4.5}$$

In this equation, H_{eff} is a non-hermitian effective Hamiltonian, and O_l stands for the jump operators related to dissipation brought on by emission into the waveguide and free space. It is important to notice that the division of the master equation into an effective Hamiltonian and jump terms is not novel; instead, our aim is to give the jump operators a physical meaning. Specifically, interference with the input light in the positive z-direction takes place when photons are emitted into the waveguide's forward-going mode. This interference, relevant to real photon detection from the waveguide, is considered in our forward-going jump operator, denoted as O_+. It can be defined as follows:

$$O_+ = \mathcal{E}_{\text{in}}(t) + i\sqrt{\frac{\Gamma_{\text{1D}}}{2}} \sum_{j} e^{-ik_0 z_j} \sigma_{\text{ge}}^{j}. \tag{4.6}$$

The backward-going jump operator, denoted as O_-, is simpler as it doesn't involve

an input field in that mode. It can be defined as:

$$O_- = i\sqrt{\frac{\Gamma_{1D}}{2}}\sum_j e^{ik_o z_j}\sigma_{ge}^j. \tag{4.7}$$

Also taken into account are the N local jump operators $O_j = \sqrt{\Gamma'}\,\sigma_{ge}^j$ related to free space decay.

By utilizing the quantum jump formalism and employing MPS, we can examine the time evolution of the spin model and capture the system's dynamics in terms of evolving pure states. This approach provides valuable insights into the behavior and properties of the considered spin model.

With the jumps formulated in this manner, the effective Hamiltonian becomes:

$$H_{\text{eff}} = H_0 - i\frac{\Gamma_{1D}}{2}\sum_{j,l=1}^{N}\exp\left(ik_0\left|z_j - z_l\right|\right)\sigma_{eg}^j\sigma_{ge}^l - \sqrt{\frac{\Gamma_{1D}}{2}}\varepsilon_{\text{in}}\left(t\right)\sum_{j=1}^{N}e^{ik_0 z_j}\sigma_{eg}^j - \frac{i}{2}\left|\varepsilon_{\text{in}}\left(t\right)\right|^2. \tag{4.8}$$

In general, any further atomic evolution is described by H_0. In the frame rotating with the input frequency for the case of two-level atoms coupled to a probe frequency ω_p, we may write,

$$H_0 = -\sum_{j=1}^{N}\left(\Delta + i\Gamma'/2\right)\sigma_{ee}^j, \tag{4.9}$$

where $\Delta = \omega_p - \omega_{eg}$.

The master equation is broken down in the quantum jump method to describe the evolution of the density operator as a sum of pure state-only trajectory sums. The stochastic nature of the system's evolution is captured by these trajectories. The deterministic development across a time step δt, starting from a pure state $|\psi(t)\rangle$ at time t, is given by:

$$|\psi(t+\delta t)\rangle = e^{-iH_{\text{eff}}\delta t}|\psi(t)\rangle. \tag{4.10}$$

During this deterministic evolution, the state's norm decreases due to the neglected effect of the jump operators which is stochastically taken into account in the quantum jump approach. A random number r between 0 and 1 is produced at the end of each deterministic evolution. The system continues in the condition $|\psi(t+\delta t)\rangle$ if $r > \delta p$. Otherwise, the state experiences a random quantum jump with the probability $\delta p_l = \delta t\langle\psi(t)|\ O_l^\dagger O_l|\psi(t)\rangle$ to the state $O_l|\psi(t)\rangle$. After normalization, the process is repeated for the next time step, generating a new quantum trajectory. By averaging the values of observables over many trajectories, we obtain the

expected values of those observables.

Furthermore, in the quantum jump approach, we select jump operators that correspond to physical processes, enabling us to interpret the distribution of jumps as representative of actual photon detection in an experiment. This interpretation establishes a connection between the simulated quantum trajectories and the observable outcomes that would be observed in a real experimental scenario.

4.5.2 Time evolution with MPS

The matrices labeled as $W^{\sigma'_j;\sigma_j}$ at site j possess physical indices, σ'_j and σ_j , indicating that W is an operator. When combining an MPS and an MPO, they can undergo a tensor contraction, as shown in Fig. 4.4.The new MPS produced by this contraction has a larger bond dimension. The bond dimension of the original MPS is multiplied by the bond dimension of the MPO, represented as D_W. To ensure computational feasibility, it is necessary to keep D_W small.

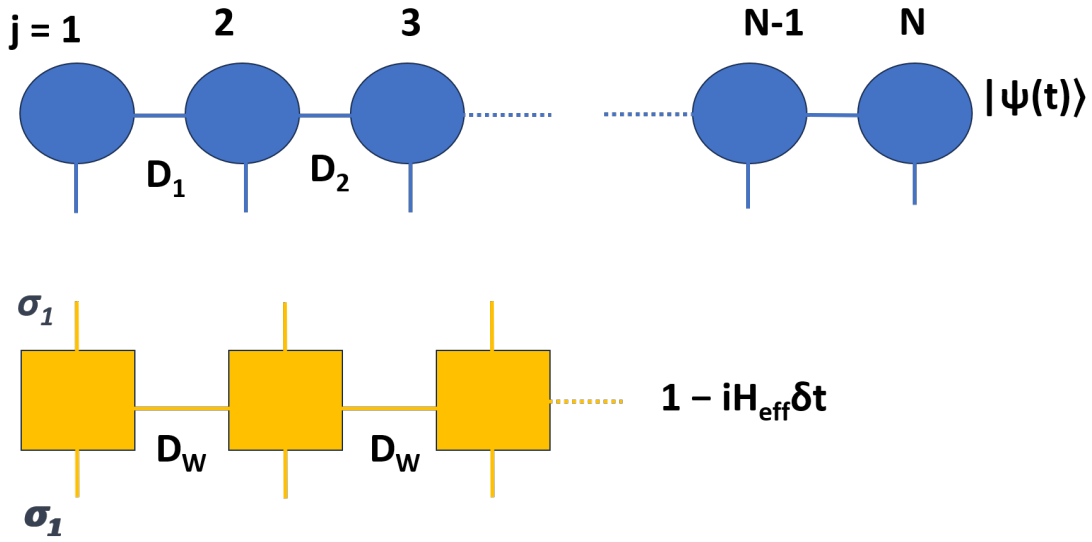

Figure 4.4: Deterministic time evolution of MPS. The initial state $|\psi(t)\rangle$ is represented in MPS form using a tensor network. The circles in the network depict local matrices A^{σ_j} on each site j, and the lines connecting them indicate the contraction of these tensors, resulting in the state $|\psi(t)\rangle$ with bond dimensions D_j. The open-ended lines correspond to the local d-dimensional Hilbert space of the atoms σ_j. The deterministic evolution is achieved by contracting these open connectors with those of the MPO representing $1 - iH_{\text{eff}}\delta t$, which are shown as a tensor network of orange squares.

While a concise representation is not currently known for the operator $e^{-iH_{\text{eff}}\delta t}$, an approximation can be made by considering the first-order term $e^{-iH_{\text{eff}}\delta t} = 1 - iH_{\text{eff}}\delta t$. If the effective Hamiltonian H_{eff} has a compact MPO form, this approximation can be expressed using such a form. This is true for the one-dimensional

spin model, where the bond dimension D_W of the effective Hamiltonian is equal to 4 in the MPO representation:

$$W_j = \begin{bmatrix} I^j & -\frac{i\lambda\Gamma_{1D}}{2}\sigma_{eg}^j & -\frac{i\lambda\Gamma_{1D}}{2}\sigma_{ge}^j & H_{loc}^j \\ 0 & \lambda I^j & 0 & \sigma_{ge}^j \\ 0 & 0 & \lambda I^j & \sigma_{eg}^j \\ 0 & 0 & 0 & I^j \end{bmatrix}, \tag{4.11}$$

Here, $\lambda = e^{ik_0 a}$, I^j stands for the identity operator for site j and H_{loc}^j contains all of the local terms in H_{eff}, Without increasing the bond dimension, the MPO of the linear expansion of the time evolution operator $1 - iH_{\text{eff}}\delta t$ is derived from this MPO. It is sufficient to replace W_1 with time evolved operator $W_1^{t.e}$:

$$W_1^{t.e} = \begin{bmatrix} -i\delta t I^1 & -\frac{\delta t\lambda\Gamma_{1D}}{2}\sigma_{eg}^1 & -\frac{\delta t\lambda\Gamma_{1D}}{2}\sigma_{ge}^1 & I^1 - i\delta t H_{loc}^1 \end{bmatrix}, \tag{4.12}$$

to obtain the desired MPO. We advance the wave function in time by applying this MPO with a small time step δt.

In the context of quantum jumps, when a system evolves for a time interval δt, the resulting state is either preserved and renormalized or a quantum jump is applied. We need an MPO representation of the jump operators that can be applied to the MPS at each time step in order to use the quantum jump formalism, as shown in Fig. 4.5. Specifically, an MPO with a bond dimension D_W of 2 is required for loss into the waveguide. The jump operator for photon emission in the +z output channel is represented as $O^+ = Z_1 \times Z_2 \times \ldots \times Z_N$ where

$$Z_j = \begin{bmatrix} I^j & i\sqrt{\frac{\Gamma_{1D}}{2}}e^{-ik_0 z_j}\sigma_{ge}^j \\ 0 & I^j \end{bmatrix} \qquad \text{for } 1 < j < N, \tag{4.13}$$

and:

$$Z_1 = \begin{bmatrix} I^1 & \varepsilon(t)I^1 + i\sqrt{\frac{\Gamma_{1D}}{2}}e^{-ik_0 z_1}\sigma_{ge}^1 \end{bmatrix}, \tag{4.14}$$

$$Z_N = \begin{bmatrix} i\sqrt{\frac{\Gamma_{1D}}{2}}e^{-ik_0 z_N}\sigma_{ge}^N & I^N \end{bmatrix}^T. \tag{4.15}$$

The MPO representation of the operator O^- follows a similar structure but with some modifications. Specifically, in the MPO for O^-, the external field term in Z_1 is omitted, and the parameter k_0 is replaced by $-k_0$. These adjustments ensure that the MPO accurately represents the desired operator O^- without the external field contribution and with the appropriate substitution of k_0 with its negative counterpart.

The size of the MPS tends to grow when jump operators are applied because

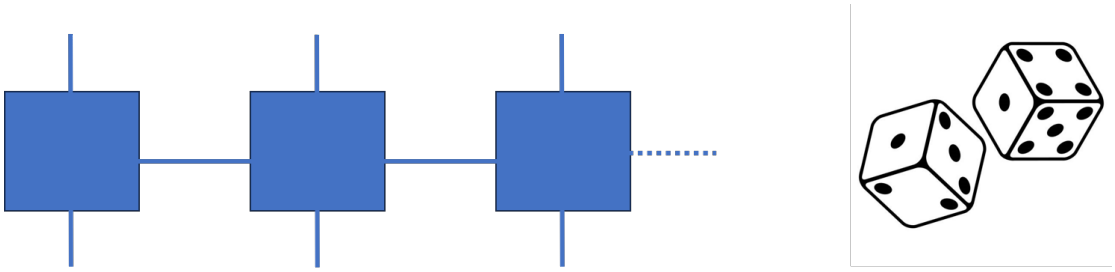

Figure 4.5: Stochastic jump matrix product operator.

the bond dimension of the operator and the bond dimension of the initial state are multiplied. If unchecked, this growth would cause the MPS size to rise exponentially over time. While this growth in bond dimension may signify actual entanglement accumulation, it may simply be the result of an ineffective MPS form manifestation of the newly discovered state. As shown in Fig. 4.6, it is conceivable to compress the bond dimension in the latter instance in order to achieve a more effective representation. Singular value decompositions are used to produce low-rank approximations of the matrices $A^{\sigma j}$ within the MPS representation in order to achieve this compression. Alternately, one can use variational methods to investigate the space of MPS states that are closest to the initial state with a fixed bond dimension. Examining how much the state's deleted parts add to the overall description might help determine the veracity of such compression. By using this evaluation, an error can be calculated, and the bond dimension in the compression can be changed in order to maintain a minimal error.

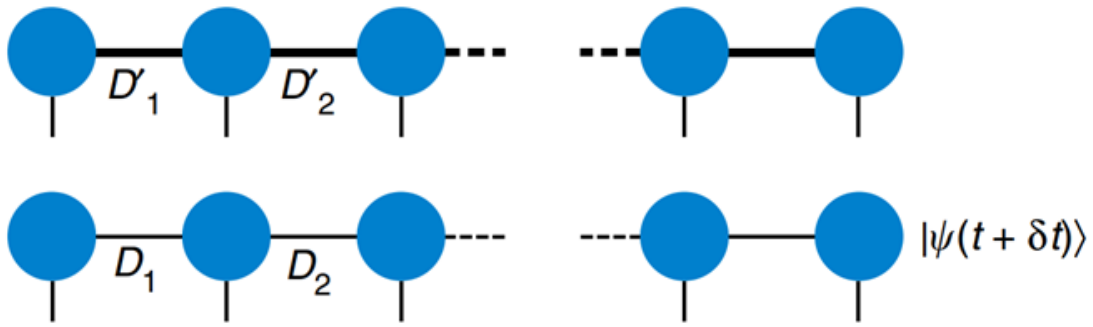

Figure 4.6: Compression of MPS resulting in lower bond dimension.

The corresponding operator associated with that observable in MPO form is applied to the state to calculate the observables for a specific quantum trajectory at any time point, such as spin populations or output field quantities. Individual elements are expressed as matrix product states or operators, for instance, to calculate the output intensity, $\langle\psi(t)|E^{\dagger}_{\text{out}}(t)E_{\text{out}}(t)|\psi(t)\rangle$. A tensor contraction, as shown in Fig. 4.7, can be used to assess the intensity for that specific trajectory. The expected value is then calculated by averaging this intensity over all quantum

paths,

$$I_{\text{out}}(t) = <E^{\dagger}_{\text{out}}(t)E_{\text{out}}(t)>. \tag{4.16}$$

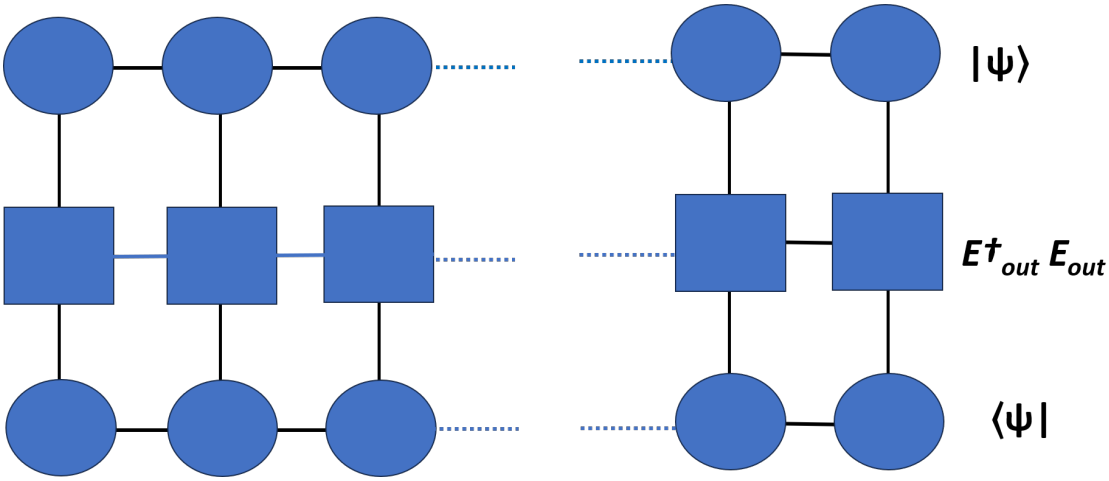

Figure 4.7: Measurement of observables.

Moreover, multi-time correlation functions can also be computed, such as

$$I^{(2)}_{\text{out}}(t, t+\tau) = <E^{\dagger}_{\text{out}}(t)E^{\dagger}_{\text{out}}(t+\tau)E_{\text{out}}(t+\tau)E_{\text{out}}(t)>. \tag{4.17}$$

This involves time evolution of state until it reaches time t, at which point the operator E_{out} is applied to the state. The operator is then applied once again after the state has evolved for an additional τ seconds. The two-time correlation is then calculated by averaging the norm of the generated states over numerous such evolutions.

4.5.3 VIT Matrix Product Operators

In order to represent VIT Hamiltonian as an MPO, an expansion of the bare spin model discussed earlier is necessary. To accommodate the additional cavity degree of freedom, an extra site is introduced in the spin chain, positioned at $N+1$. By augmenting the bare representation with two additional columns and rows, the MPO of H_{eff} for the VIT case is obtained. These additional elements account for the inclusion of the cavity degree of freedom, resulting in an expanded MPO representation that incorporates the VIT Hamiltonian.

For $0 < j < N$, the MPO representation $W_{\mathrm{VIT}}(j)$ is given by:

$$W_{\mathrm{VIT}}(j) = \begin{pmatrix} \ldots & \ldots & \ldots & \frac{g}{2}\sigma^j_{\mathrm{es}} & \frac{g}{2}\sigma^j_{\mathrm{se}} & \ldots \\ \ldots & \ldots & \ldots & 0 & 0 & \ldots \\ \ldots & \ldots & \ldots & 0 & 0 & \ldots \\ 0 & 0 & 0 & I^j & 0 & 0 \\ 0 & 0 & 0 & 0 & I^j & 0 \\ \ldots & \ldots & \ldots & 0 & 0 & \ldots \end{pmatrix}. \quad \text{for } 0 < j < N \tag{4.18}$$

Additionally, for the $N+1$ site, the corresponding MPO element is:

$$W^{\mathrm{VIT}}_{N+1} = \begin{pmatrix} H_{\mathrm{loc,cav}} & 0 & 0 & b & b^\dagger & I_{\mathrm{cav}} \end{pmatrix}^T. \tag{4.19}$$

4.6 Convergence and accumulated error

During the time evolution of MPS, it is observed that the bond dimension of the MPS tends to grow. Specifically, when the time evolution MPO is applied to an MPS with a maximum bond dimension of D, using a maximum bond dimension of D_W for the MPO, the resulting MPS bond dimension becomes $D' = D_W \times D$. It is usual practise in simulations to keep the maximal bond dimension D constant throughout the evolution. The MPS must be carefully compressed from dimension D' to D after each step in order to do this. This compression enables efficient computation while ensuring that important information from the state is not discarded.

Chapter 5

Results and Discussion

In the simulation of VIT using the MPS method, specific considerations are made for analyzing system's dynamics. The input pulses are characterized by a Gaussian envelope with a central frequency ω_p and a width parameter σ_t. The pulse shape is described by the function:

$$\xi_{\text{in}}(t) = \alpha \left(\frac{\pi\sigma_t^2}{2}\right)^{1/4} \exp\left(-\frac{(t-t_0)^2}{\sigma_t^2}\right), \tag{5.1}$$

where α represents the pulse amplitude, and t_0 is the central time of the pulse. Average photon number is given as $< n_{\text{pulse}} >= |\alpha|^2$=1. Keeping in mind the expected properties of the delay of fock states in VIT, we devise an ideal toy model where a coherent state is input and output is calculated by delaying the input fock state n by time t_n=L/v_n and assuming no losses. In an idealized scenario, a coherent pulse with an average of one photon is transmitted through a VIT medium. Assuming no losses and no pulse distortion on entry and exit, the individual components of the input pulse propagate with group velocity $v_n \propto n$. This results (shown in Fig.5.1) in the separation of one photon (purple), two photon (green), and three photon (red) components in the output field. The parameters used are $v_1 = 4\text{a}\Gamma'$ and the medium length L = 100a.

The MPS simulation yields an output intensity $I_{\text{out}}(t)$ that displays two prominent peaks as shown in Fig. 5.2 and Fig. 5.3. Photon number components with two or more photons corresponds to the initial peak, which was seen at time $t\Gamma' \approx 23$. The sluggish escape of the single-photon component is represented by the second peak, which appears at $t\Gamma' \approx 36$. This behavior aligns with the expected group velocities for different photon numbers, as illustrated in Fig. 5.1.

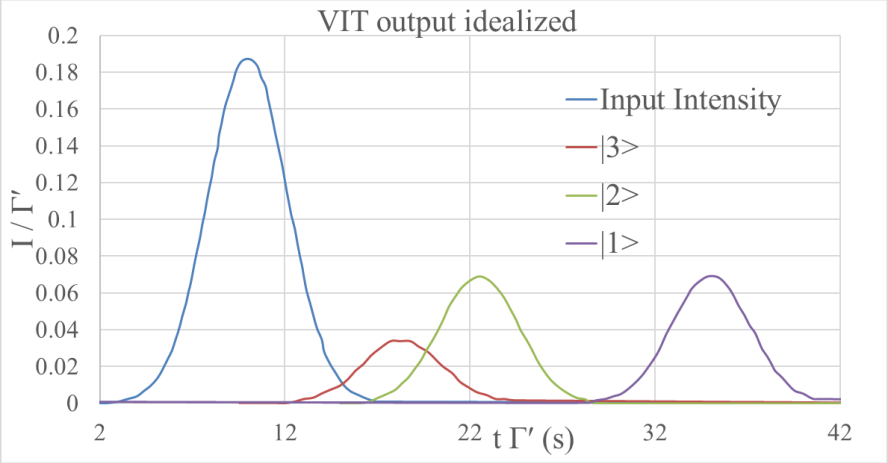

Figure 5.1: Ideal temporal evolution of a coherent pulse in transmission where a coherent state with $|\alpha|^2$=1 is input and no losses are assumed resulting in a clean separation of input fock states.

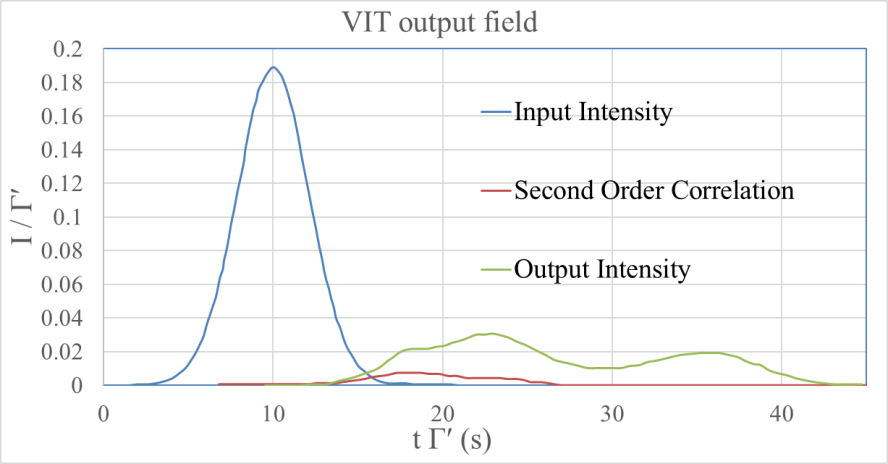

Figure 5.2: Pulse propagation simulation in a VIT medium at an optical depth of 400. This study averages 20000 quantum trajectories with $N = 100$ atoms coupled to a 1D waveguide. The figure displays the output intensity $I_{\text{out}}(t)$ and the second-order correlation function (red) for a coherent pulse input with $|\alpha|^2 = 1$ (blue), which reveals two main peaks.

To further analyze the output intensity, the second-order correlation function

$$I^{(2)}_{\text{out}}(t,t) \equiv \left\langle E^{\dagger}_{\text{out}}(t) E^{\dagger}_{\text{out}}(t) E_{\text{out}}(t) E_{\text{out}}(t) \right\rangle \tag{5.2}$$

is examined. The correlation function is only non-zero in the first portion of the output pulse, as seen in Fig. 5.3, indicating the presence of single photons there.

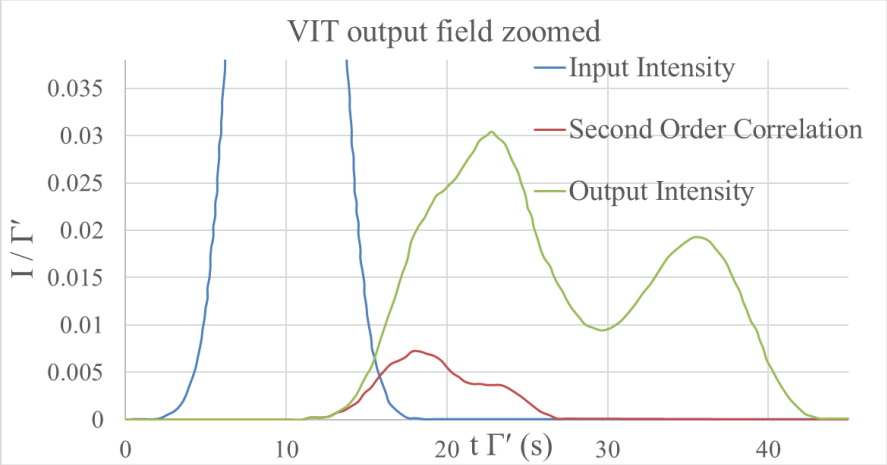

Figure 5.3: Zoomed-in plot of Fig. 5.2.

When comparing the ideal scenario depicted in Fig. 5.1 with the full MPS simulation Fig. 5.2, a higher intensity between the one-photon and two-photon peaks is noticed in the simulation. This difference is attributed to the influence of quantum jumps, which blur the distinction between different photon number components in the output. Single photons tend to reach the output earlier than expected even with favourable system parameters like high optical depth (OD = 400) and strong coupling ($g/\kappa \approx 130$) due to the occurrence of quantum jumps. This is due to the possibility of two-photon components decaying to a single photon during the evolution, leading to a change in the group velocity. As a result, the perfect separation between the two-photon component and single-photon output is hampered.

By analyzing the MPS trajectories and comprehending the effects of quantum jumps, valuable insights into the underlying physics of VIT can be gained. Despite the blurring of photon number components in the output, the simulation results still capture the key characteristics of VIT, including the delayed propagation and separation of single photons from higher photon number components.

To quantitatively evaluate the observed behavior in our simulations, an analysis of the quantum jumps is conducted. These jumps can be understood by considering the chosen physical jump operators, which were elaborated in Section 4.5. They allow us to create a link between the number of photons released from the system and the total number of jumps along a trajectory. We can also distinguish between distinct jump kinds, such as those caused by cavity loss, free-space loss or detection in the waveguide output. A histogram showing the average number of jumps into the waveguide output channel over time is shown in Fig. 5.4. This data is derived from the 20,000 trajectories used to generate Fig. 5.2. The histogram serves as an alternative approach to calculate intensity, akin to meth-

ods employed in experimental settings where detector counts are averaged across multiple realizations.

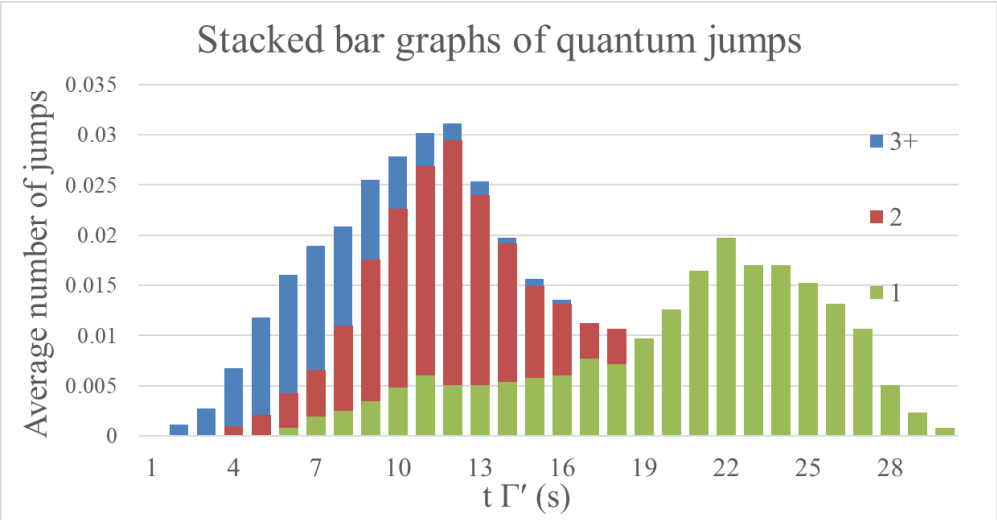

Figure 5.4: Visualizing quantum jumps in the output channel: Stacked bar graph analysis across 20,000 Quantum trajectories, provides a visual representation of the quantum jumps observed.

The plot's bars are color-coded to show leaps coming from paths with 1, 2, or 3+ photons that were emitted into the waveguide. It is evident from the plot that jumps occurring earlier in time are associated with a higher photon number detected in the waveguide. This observation aligns with the predictions of the theoretical model in Section 4.4 and the calculations of $I_{\text{out}}(t)$ and $I^{(2)}_{\text{out}}(t,t)$ in Fig. 5.2.

Let's focus on paths where a single photon is found at the waveguide output to dive deeper. Within this subset, there are two types of situations that can be distinguished: (i) those in which the jump event is the only one, signifying the successful propagation of a single photon through the system; and (ii) those in which a multi-photon state was initially input but all but one photon decayed into other channels. A histogram based on this classification over time is shown in Fig. 5.5. The plot shows that faster arriving single photons are caused by the decay of higher photon number states and the consequent mixing of propagation velocities, which is observed to the left of the main peak.

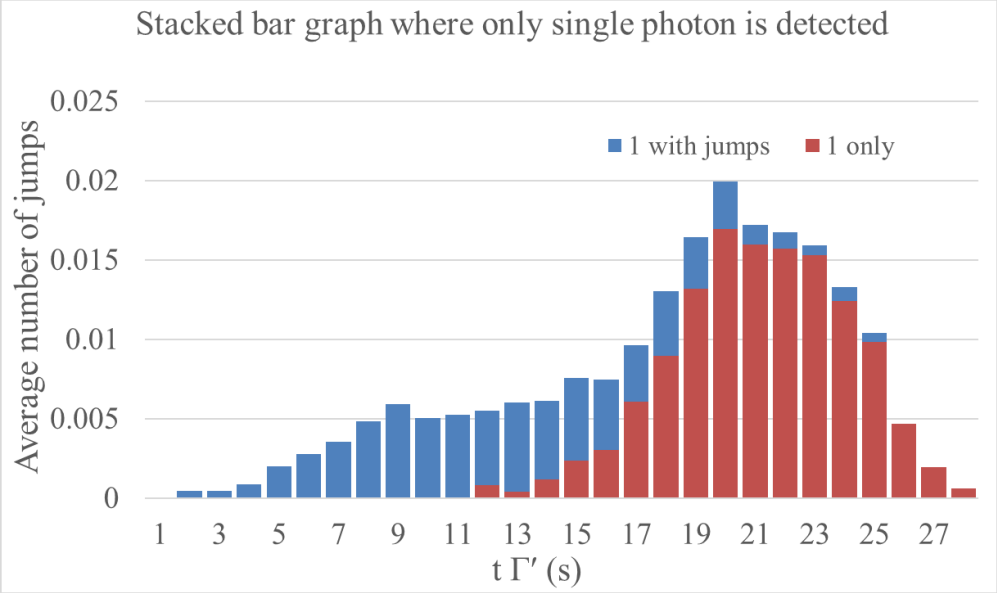

Figure 5.5: Visualization of stacked bar graph for single photon detection in quantum trajectories from the waveguide output.

Jump statistics from a coherent state input can also be used to estimate the intensity resulting from a fock state input. The total number of photons that jump out of the VIT system for a particular trajectory equals the total number of photons that entered the system since long-lived excitations are missing on the simulated time scale. As shown in Fig. 5.6, we can extract the intensity resulting from a fock state input by selectively analysing trajectories depending on the total number of jumps. This analysis highlights similar impact of jumps observed previously but from a different perspective. While Fig. 5.4 and Fig. 5.5 classified trajectories according to how many photons survive and are output, Fig. 5.6 categorises them according to how many photons are entered. Again as a result of loss of photons and propagation speed mixing, the output intensities for fock state inputs with two or more photons show larger delay durations than anticipated.

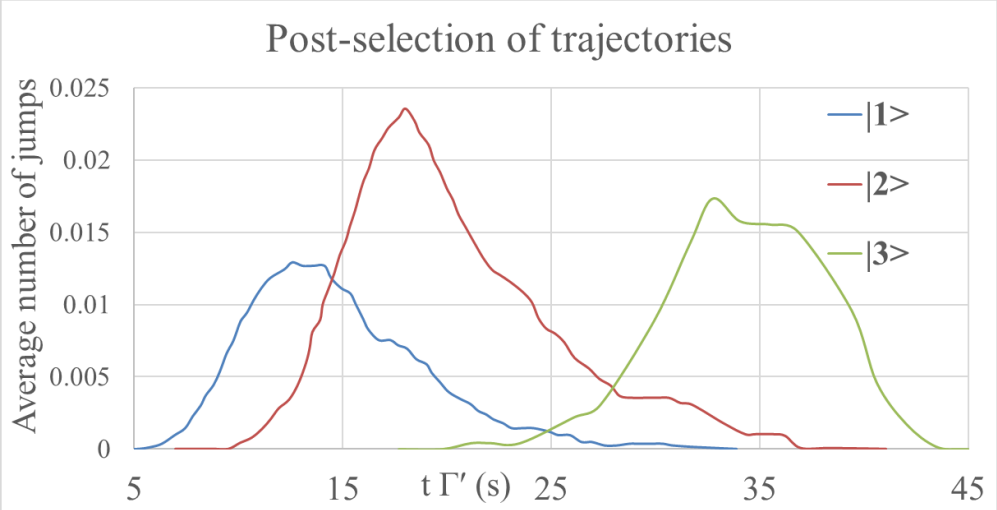

Figure 5.6: Selective trajectory post-selection for analyzing the evolution of fock state inputs, depicts the process of selectively analyzing trajectories based on the total number of jumps to examine the evolution of fock state inputs.

It's crucial to note that quantum jumps are not the only cause of the delay seen in the output. They may also result from the multi-photon wavepacket's deformation once it has entered the medium. As the input pulse reaches the atomic ensemble's border, this distortion happens. The two photons may arrive at the atomic ensemble's boundary at different moments when the two-photon wave function has the shape of a Gaussian pulse. Up until the second photon enters, which causes the group velocity to change to $2v_1$, the first photon entering moves at velocity v_1. The photons' process of leaving the medium is similar. As a result, greater photon delays result from a larger spacing between the photons in the original pulse. Due to this phenomena, higher photon number manifolds display higher-dimensional heart forms and the Gaussian-shaped two-photon input is distorted into a heart-shaped output. This behaviour is shown in Fig. 5.7 in the two-time correlation measurement of the output photons for a coherent pulse with a low input photon number. Due to the presence of higher photon number manifolds with faster group velocities that smear out the distribution as the input photon number rises, the heart shape becomes even more deformed.

Plots of the output intensity and zero-delay second-order correlation function for various bond dimensions are shown in Fig. 5.8 and Fig. 5.9 in a trajectory without jumps. These plots show convergence behaviour in the VIT example using the Fig. 5.2 parameters. The intensity shows good convergence already at $D = 20$, while for the convergence of zero-delay second-order correlation function, a higher bond dimension of around $D \sim 50$ is required. The fact that the higher-number components of the pulse are given more weight in the second-order correlation function suggests that a bigger bond dimension is necessary for correct modelling

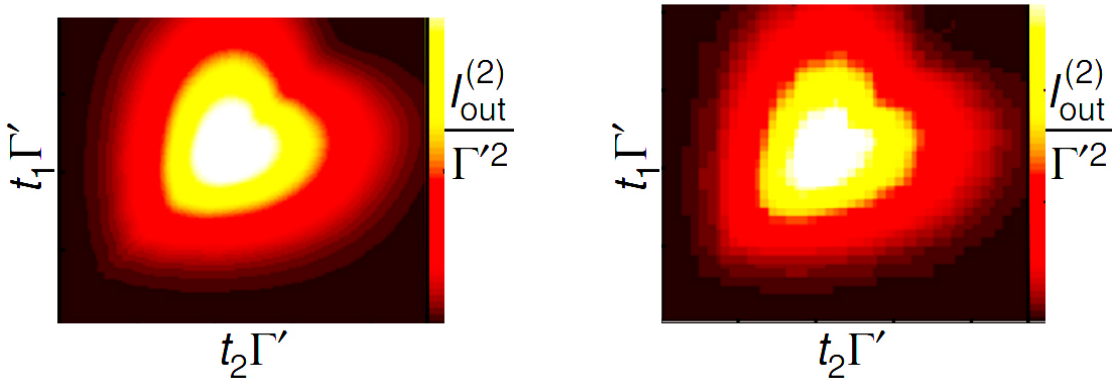

(a) $|\alpha|^2 = 0.01$ (b) $|\alpha|^2 = 0.25$

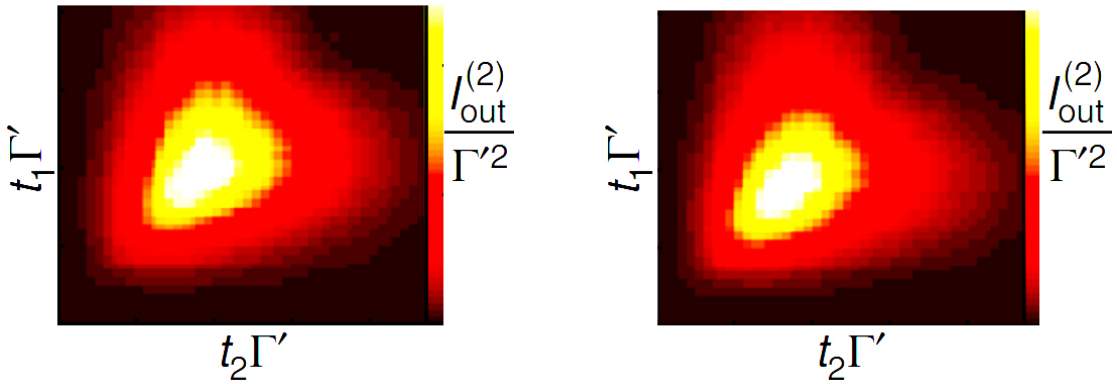

(c) $|\alpha|^2 = 1$ (d) $|\alpha|^2 = 2$

Figure 5.7: Analysis of two-time correlation function $I^2_{\text{out}}(t_1, t_2)$ in the output field of the VIT System with coherent gaussian input pulse at different average input photon numbers $|\alpha|^2$.

of these components. As a result, the bond dimension in simulations is set to $D = 50$.

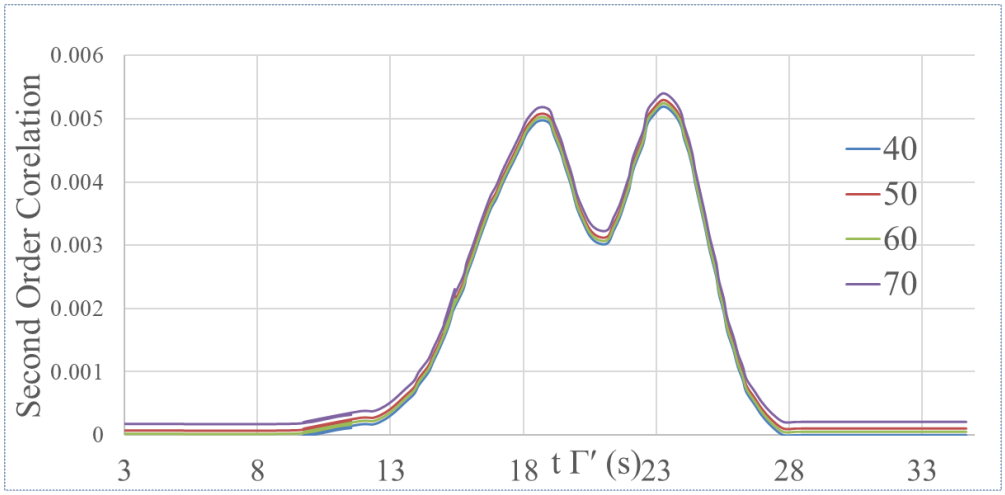

Figure 5.8: The intensity convergence in VIT is studied for a jump-free quantum trajectory at different maximum bond dimensions (D) in MPS simulations.

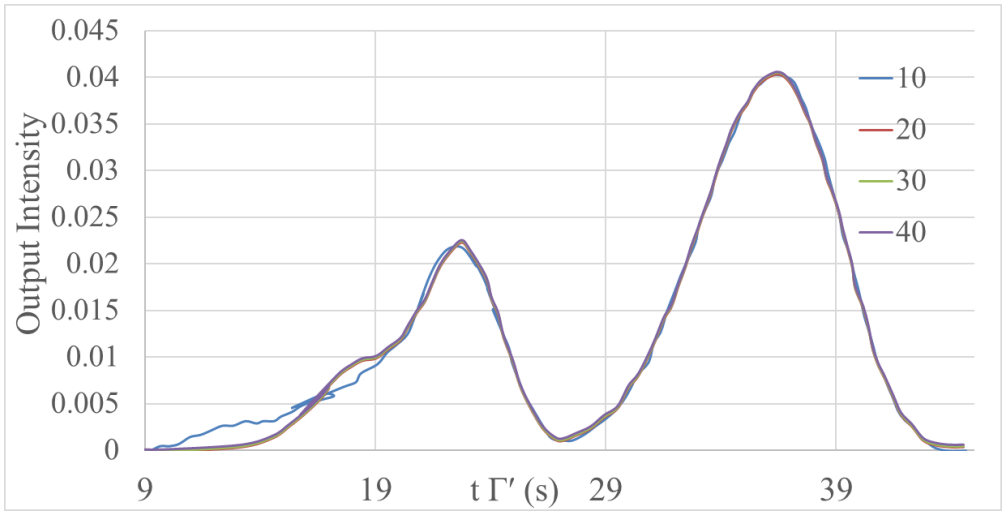

Figure 5.9: The zero-delay second-order correlation function in VIT is examined for a jump-free quantum trajectory at varying maximum bond dimensions (D).

It's crucial to keep an eye on the inaccuracy generated by each compression phase to make sure the simulations faithfully reflect physical reality. A sequence of SVD's of the bond connections between each site can be used to compress data by minimising the difference between the larger MPS $|\psi(t)\rangle_{D'}$ and its compressed version $|\psi(t)\rangle_D$. The difference between the original state and the compressed state's norm may be used to calculate the compression error ϵ_tot $= |||\psi(t)\rangle_D - |\psi(t)\rangle_{D'}||$. By taking into account the unique values that were rejected, this inaccuracy can be roughly estimated. As bond dimension grows, the inaccuracy decreases, as seen in Fig. 5.10. This leads us to the conclusion that by increasing the bond dimension D, the error can be made to be of any size.

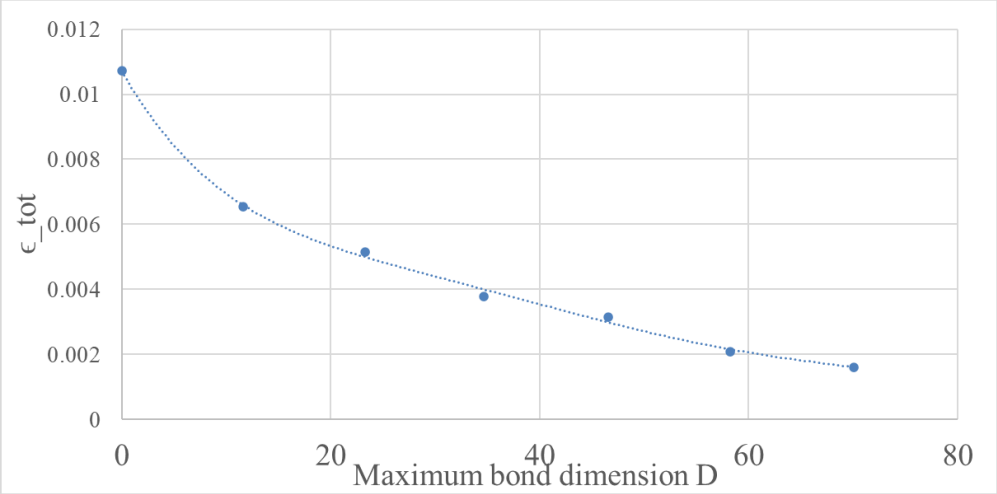

Figure 5.10: The logarithmic-scale accumulated compression error ϵ_tot is analyzed against the maximum bond dimension (D) in MPS simulations, providing insights into the trade-off between computational efficiency and accuracy in VIT simulations.

Conclusions

In summary, our analysis of the simulations involves examining the behavior of the system by quantifying quantum jumps. Through the analysis of the number and types of jumps, we gain valuable insights into the emitted photons and their characteristics. To calculate the intensity and understand the dynamics of single and multi-photon states, we utilize histograms as alternative approaches, as depicted in Fig. 5.4 and Fig. 5.5. Furthermore, Fig. 5.6 presents a different perspective by considering jump statistics from an input of a coherent state. It is important to note that the observed delay times are influenced not only by quantum jumps but also by the distortion of multi-photon wavepackets upon entering the medium. This distortion arises from the variations in arrival times of photons at the boundary of the atomic ensemble, resulting in complex output shapes.

In addition to these findings, the use of MPS and Tensor Network techniques enables us to perform numerical simulations. These computational methods contribute to the analysis and understanding of the system's behavior. The ability to classify and analyze quantum jumps, along with the utilization of MPS and Tensor Network, enhances our knowledge and insights in the field of quantum physics research. These findings have significant implications for experimental settings and provide valuable contributions to advancing our understanding of quantum phenomena.

Bibliography

[1] M. T. Manzoni, D. E. Chang, and J. S. Douglas, "Simulating quantum light propagation through atomic ensembles using matrix product states," *Nature Communications*, vol. 8, no. 1, p. 1743, 2017.

[2] P. A. M. Dirac, "The quantum theory of the electron," *Proceedings of the Royal Society of London. Series A, Containing Papers of a Mathematical and Physical Character*, vol. 117, no. 778, pp. 610–624, 1928.

[3] J. Eisert, M. Cramer, and M. B. Plenio, "Colloquium: Area laws for the entanglement entropy," *Reviews of modern physics*, vol. 82, no. 1, p. 277, 2010.

[4] U. Schollwöck, "The density-matrix renormalization group," *Reviews of modern physics*, vol. 77, no. 1, p. 259, 2005.

[5] Y. Saad, "On the rates of convergence of the Lanczos and the block-Lanczos methods," *SIAM Journal on Numerical Analysis*, vol. 17, no. 5, pp. 687–706, 1980.

[6] C. Wentworth and Y.-L. Wang, "Linked-cluster series-expansion technique for quantum spin systems," *Physical Review B*, vol. 36, no. 16, p. 8687, 1987.

[7] G. Kotliar, S. Y. Savrasov, K. Haule, V. S. Oudovenko, O. Parcollet, and C. A. Marianetti, "Electronic structure calculations with dynamical mean-field theory," *Reviews of Modern Physics*, vol. 78, no. 3, p. 865, 2006.

[8] C.-C. Lin, F. H. Zong, and D. M. Ceperley, "Twist-averaged boundary conditions in continuum quantum monte carlo algorithms," *Physical Review E*, vol. 64, no. 1, p. 016702, 2001.

[9] H. Krull, N. A. Drescher, and G. S. Uhrig, "Enhanced perturbative continuous unitary transformations," *Physical Review B*, vol. 86, no. 12, p. 125113, 2012.

[10] Y. Bomble, J. Stanton, M. Kállay, and J. Gauss, "Coupled-cluster methods including noniterative corrections for quadruple excitations," *The Journal of chemical physics*, vol. 123, no. 5, p. 054101, 2005.

[11] M. Orio, D. Pantazis, and F. Neese, "Density functional theory," *Photosynthesis research*, vol. 102, pp. 443–453, 2009.

[12] I. Arad and Z. Landau, "Quantum computation and the evaluation of tensor networks," *SIAM J. Comput.*, vol. 39, no. 7, pp. 3089–3121, 2010.

[13] F. Mila, "Quantum spin liquids," *Eur. J. Phys.*, vol. 21, no. 6, p. 499, 2000.

[14] R. Orús, T.-C. Wei, O. Buerschaper, and M. Van den Nest, "Geometric entanglement in topologically ordered states," *New Journal of Physics*, vol. 16, no. 1, p. 013015, 2014.

[15] H. Tanji-Suzuki, W. Chen, R. Landig, J. Simon, and V. Vuletić, "Vacuum-induced transparency," *Science*, vol. 333, no. 6047, pp. 1266–1269, 2011.

[16] J. Glattfelder, "A universe built of information," in *Information—Consciousness—Reality: How a New Understanding of the Universe Can Help Answer Age-Old Questions of Existence*, pp. 473–514, Springer, 2019.

[17] J. Eisert, M. Cramer, and M. B. Plenio, "Area laws for the entanglement entropy-a review," *Reviews of Modern Physics*, vol. 82, no. 1, pp. 277–306, 2010.

[18] H. D. Simon, "The Lanczos algorithm with partial reorthogonalization," *Mathematics of computation*, vol. 42, no. 165, pp. 115–142, 1984.

[19] Y. Zhou and Y. Saad, "A Chebyshev–Davidson algorithm for large symmetric eigenproblems," *SIAM Journal on Matrix Analysis and Applications*, vol. 29, no. 3, pp. 954–971, 2007.

[20] I. Dhand and B. C. Sanders, "Stability of the trotter–suzuki decomposition," *Journal of Physics A: Mathematical and Theoretical*, vol. 47, no. 26, p. 265206, 2014.

[21] S. Singh, R. N. Pfeifer, and G. Vidal, "Tensor network states and algorithms in the presence of a global U (1) symmetry," *Physical Review B*, vol. 83, no. 11, p. 115125, 2011.

[22] S. Singh and G. Vidal, "Tensor network states and algorithms in the presence of a global SU (2) symmetry," *Physical Review B*, vol. 86, no. 19, p. 195114, 2012.

[23] G. Vidal, "Tensor network renormalization." Introduced by John Preskill. 2006-2008 DuBridge Fellow, 2003-2005 Sherman Fairchild Fellow, Senior Faculty, Perimeter Institute for Theoretical Physics, Waterloo.

[24] J. Latorre and A. Riera, "A short review on entanglement in quantum spin systems," *Journal of physics a: mathematical and theoretical*, vol. 42, no. 50, p. 504002, 2009.

[25] C.-K. Hu, "Historical review on analytic, monte carlo, and renormalization group approaches to critical phenomena of some lattice models," *Chinese Journal of Physics*, vol. 52, no. 1, pp. 1–76, 2014.

[26] I. Jack and H. Osborn, "Constraints on RG flow for four dimensional quantum field theories," *Nuclear Physics B*, vol. 883, pp. 425–500, 2014.

[27] R. Haghshenas, J. Gray, A. C. Potter, and G. K.-L. Chan, "Variational power of quantum circuit tensor networks," *Physical Review X*, vol. 12, no. 1, p. 011047, 2022.

[28] S.-H. Li and L. Wang, "Neural network renormalization group," *Physical Review Letters*, vol. 121, no. 26, p. 260601, 2018.

[29] V. Bužek and M. Hillery, "Quantum disentanglers," *Physical Review A*, vol. 62, no. 5, p. 052303, 2000.

[30] L. Cincio, J. Dziarmaga, and M. M. Rams, "Multiscale entanglement renormalization ansatz in two dimensions: quantum Ising model," *Physical Review Letters*, vol. 100, no. 24, p. 240603, 2008.

[31] D. Volchenkov, "Renormalization group and instantons in stochastic nonlinear dynamics: From self-organized criticality to thermonuclear reactors," *The European Physical Journal Special Topics*, vol. 170, no. 1, pp. 1–142, 2009.

[32] S. R. White, "Density matrix formulation for quantum renormalization groups," *Physical Review Letters*, vol. 69, no. 19, p. 2863, 1992.

[33] G. Evenbly and G. Vidal, "Tensor network renormalization," *Physical review letters*, vol. 115, no. 18, p. 180405, 2015.

[34] G. Evenbly and G. Vidal, "Algorithms for entanglement renormalization: Boundaries, impurities and interfaces," *Journal of Statistical Physics*, vol. 157, no. 4-5, pp. 931–978, 2014.

[35] A. Karch, Z.-X. Luo, and H.-Y. Sun, "Holographic duality for Ising CFT with boundary," *Journal of High Energy Physics*, vol. 2021, no. 4, pp. 1–24, 2021.

[36] B. Swingle, "Constructing holographic spacetimes using entanglement renormalization," *arXiv:1209.3304*, 2012.

[37] D. Harlow, "The Ryu-Takayanagi formula from quantum error correction," *Communications in Mathematical Physics*, vol. 354, no. 3, pp. 865–912, 2017.

[38] G. Evenbly, "Hyperinvariant tensor networks and holography," *Physical Review Letters*, vol. 119, no. 14, p. 141602, 2017.

[39] A. Browaeys and T. Lahaye, "Many-body physics with individually controlled rydberg atoms," *Nature Physics*, vol. 16, pp. 132–142, 2020.

[40] X. Wang, T. Hiroshima, A. Tomita, and M. Hayashi, "Quantum information with gaussian states," *Physics Reports*, vol. 448, no. 1-4, pp. 1–111, 2007.

[41] D. Browne, J. Eisert, S. Scheel, and M. Plenio, "Driving non-gaussian to gaussian states with linear optics," *Physical Review A*, vol. 67, no. 6, p. 062320, 2003.

[42] K. Birnbaum, A. Boca, R. Miller, A. Boozer, T. Northup, and H. Kimble, "Photon blockade in an optical cavity with one trapped atom," *Nature*, vol. 436, no. 7047, pp. 87–90, 2005.

[43] A. N. Poddubny, "Quasiflat band enabling subradiant two-photon bound states," *Physical Review A*, vol. 101, no. 4, p. 043845, 2020.

[44] M. H. Devoret, A. Wallraff, and J. M. Martinis, "Superconducting qubits: A short review," *arXiv:0411174*, 2004.

[45] M. A. Reed, "Quantum dots," *Scientific American*, vol. 268, no. 1, pp. 118–123, 1993.

[46] E. Shahmoon, P. Grišins, H. P. Stimming, I. Mazets, and G. Kurizki, "Highly nonlocal optical nonlinearities in atoms trapped near a waveguide," *Optica*, vol. 3, no. 7, p. 725, 2016.

[47] J. S. Douglas, T. Caneva, and D. E. Chang, "Photon molecules in atomic gases trapped near photonic crystal waveguides," *Physical Review X*, vol. 6, no. 3, p. 031017, 2016.

[48] D. Chang, V. Gritsev, G. Morigi, V. Vuletić, M. Lukin, and E. Demler, "Crystallization of strongly interacting photons in a nonlinear optical fibre," *Nature Physics*, vol. 4, no. 11, pp. 884–889, 2008.

[49] T. Caneva, M. T. Manzoni, T. Shi, J. S. Douglas, J. I. Cirac, and D. Chang, "Quantum dynamics of propagating photons with strong interactions: a generalized input–output formalism," *New Journal of Physics*, vol. 17, no. 11, p. 113001, 2015.

[50] Y. Castin, K. Mo, *et al.*, "Maxwell-bloch equations: A unified view of nonlinear optics and nonlinear atom optics," *Physical Review A*, vol. 51, no. 5, p. R3426, 1995.

[51] I. P. McCulloch, "From density-matrix renormalization group to matrix product states," *Journal of Statistical Mechanics: Theory and Experiment*, vol. 2007, no. 10, p. P10014, 2007.

[52] S. Mahmoodian, G. Calajó, D. E. Chang, K. Hammerer, and A. S. Sørensen, "Dynamics of many-body photon bound states in chiral waveguide QED," *Physical Review X*, vol. 10, no. 3, p. 031011, 2020.

[53] N. Lauk and M. Fleischhauer, "Number-state filter for pulses of light," *Physical Review A*, vol. 93, no. 6, p. 063818, 2016.

[54] G. Nikoghosyan and M. Fleischhauer, "Photon-number selective group delay in cavity induced transparency," *Physical Review Letters*, vol. 105, no. 1, p. 013601, 2010.